Zeitschrift: Schweizerische mineralogische und petrographische Mitteilungen = Bulletin suisse de minéralogie et pétrographie

Band: 81 (2001)

Heft: 3: Monte Rosa nappe

Artikel: Metamorphic evolution of pelitic rocks of the Monte Rosa nappe : constraints from petrology and single grain monazite age data

Autor: Engi, Martin / Scherrer, Nadim C. / Burri, Thomas

DOI: https://doi.org/10.5169/seals-61695

SCHWEIZ. MINERAL. PETROGR. MITT. 81, 305–328, 2001

Metamorphic evolution of pelitic rocks of the Monte Rosa nappe: Constraints from petrology and single grain monazite age data

by *Martin Engi*[1], *Nadim C. Scherrer*[1] and *Thomas Burri*[1]

Abstract

A suite of metapelites from the pre-granitic basement of the Monte Rosa nappe was collected and investigated to gain insight into the evolution of this important upper Penninic thrust sheet. Careful sampling at mesoscopic to microscopic scale allowed the identification of relics of distinctly pre-Alpine origin, of assemblages formed in the early Alpine high pressure history of the nappe, and of features due to the Meso-Alpine thermal overprint. Variscan structural relics, e.g. large monazite grains with relic cores, or monazite inclusions within garnet porphyroblasts, were recognized in the field and at thin section scale. Alpine features include high pressure and younger thermal phases; these are not readily separable in the field, but they are usually distinctly identifiable at thin section scale.

Combined chemical Th–U–Pb dating of monazite by electron microprobe and novel XRF-microprobe analysis, verified and enhanced by isotopic laser ablation PIMMS analysis, was performed on single monazite grains selected in thin section, with the full context information preserved. Based on electron microprobe data for assemblages from these same thin sections, TWQ thermobarometry indicates metamorphic conditions preserved along the P-T-t path of a polyorogenic evolution. In only two samples monazite inclusions in old garnet were found to record ages of 330 Ma, corresponding to the intrusion of the main Mote Rosa granodiorite mass. High-grade Permian metapelites appear variably affected – in isolated cases even unaffected – by all Alpine activity, retaining mineral assemblages, consistent P-T-information, and monazite grains (even within the sample matrix) formed some 270 Ma ago in response to the intrusion of granitic masses in the Monte Rosa nappe. This same stage of low to medium pressure metamorphism was detected in monazite inclusions in garnet from numerous samples taken at various localities. Reaching sillimanite+Kspar grade, this stage is evident in migmatic restites as well and is suggested to represent either a regional event, at 10–20 km depth, associated with the generation and emplacement of an extensive suite of acid dykes and small stocks; alternatively, and more or less equivalently, one may think of this phase as indicating widespread contact metamorphism.

No evidence whatsoever could be found supporting a questionable Cretaceous high-pressure phase. Consistent TWQ pressures between 9.2 ± 1.8 and 12 ± 1.5 kbar, with temperatures ranging from 595 ± 25 to 755 ± 65 °C, represent the dominant Alpine overprint documented in samples containing assemblages kyanite + garnet + phengite ± staurolite. Median conditions are 11.0 ± 1.2 kbar and 652 ± 41 °C, with no significant regional gradient, Monazite single grain dates range from 46 to 31 Ma, but with most of the accurate ages lying between 38 and 32 Ma. Several petrological observations suggest that this stage probably represents (partial) re-equilibration upon decompression, rather than the maximum depth reached by the Monte Rosa nappe. Late Alpine thermal overprinting is evidenced by only very few monazite ages of <30 Ma obtained, and no precise P-T-brackets could be obtained for that retrograde stage.

Recent paleogeographic models for the Alpine evolution derive the Monte Rosa nappe from the southern European continental margin. Our results demand that the subduction system implicated this nappe sufficiently early to yield peak metamorphic temperatures near 700 °C at 35–30 km depth in the Eocene, probably during extrusion following subduction and slab breakoff. Higher pressure relics are known from several areas along the margin of the Monte Rosa nappe, including the UHP-fragments of Lago Cignana. These relics appear to be restricted to the immediate periphery of the Monte Rosa nappe, outlining a discontinuous mantle of highly strained fragments of ophiolitic and metasedimentary trails. Whether the Furgg Zone, at least its northern parts, may also represent a tectonic mélange, is currently controversial. It seems likely that strain concentration in marginal zones of the Monte Rosa

[1] Mineralogisch-petrographisches Institut, Universität Bern, Baltzerstrasse 1, CH-3012 Bern, Switzerland. <engi@mpi.unibe.ch>

thrust sheet enabled the tectonic emplacement of the several massive granitic sheets that make up the bulk of the nappe. These were left largely intact, thus preserving pre-Alpine and early Alpine assemblages in metapelites protected within less deformed portions of the metagranitoids.

Keywords: Monte Rosa, Alps, polymetamorphism, metapelites, monazite dating, exhumation, high pressure.

1. Introduction

The Monte Rosa nappe is a classic crystalline basement nappe situated at the tectonic junction between the Central and the Western Alps. Despite impressive insights from many eminent Alpine geologists (e.g. ARGAND, 1911; BEARTH, 1939; BEARTH, 1952; DAL PIAZ, 1964; DAL PIAZ, 1966; FRANCHI, 1903; FREY et al., 1976; HUNZIKER, 1970; MATTIROLO et al., 1913; REINHARDT, 1966), the evolution and paleogeographic provenance of the Monte Rosa nappe remain controversial. It contains widespread evidence of a protracted polymetamorphic history: Voluminous Variscan granitoids intruded a high-grade gneiss basement, including deformed migmatites, causing contact metamorphism; subsequent regional metamorphism affected this complex, still during the Permian; the Alpine orogeny first produced prominent eclogites and other high-pressure rocks, followed by a widespread Barrovian overprint reaching greenschist facies in the West and amphibolite facies in the eastern portions of the nappe. In terms of tectonic position in the Alpine nappe stack, the Monte Rosa nappe (Fig. 1) lies at a level corresponding, in the West, to the Gran Paradiso and Dora Maira "massifs" and, further East, to the Adula nappe, all of which contain Alpine eclogites as well. For the Adula nappe, for example, rapid exhumation from depths in excess of 70 km during the mid Tertiary is well established (e.g. FREY and FERREIRO MÄHLMANN, 1999; NAGEL, 2000). To what extent the high pressure relics in all of these tectonic units may be interpretable in terms of one coherent subduction/emplacement history is a key question in Alpine geodynamics and is relevant in the context of collisional orogeny in general. Current understanding of the kinematic sequence of events and their thermal consequences, in particular, is certainly far from complete in any orogen, including the Alps.

Progress on these questions depends to no small degree on reliable *temporal* links between several stages of evolution documented by petrological and structural studies for each of these units. For the Monte Rosa nappe, petrographic work by BEARTH (1952, 1958) and DAL PIAZ (1971) documented that, due to localized strain within the nappe, plurifacial assemblages are not just locally preserved, but occur in several km^2-size domains. Previous efforts to constrain the

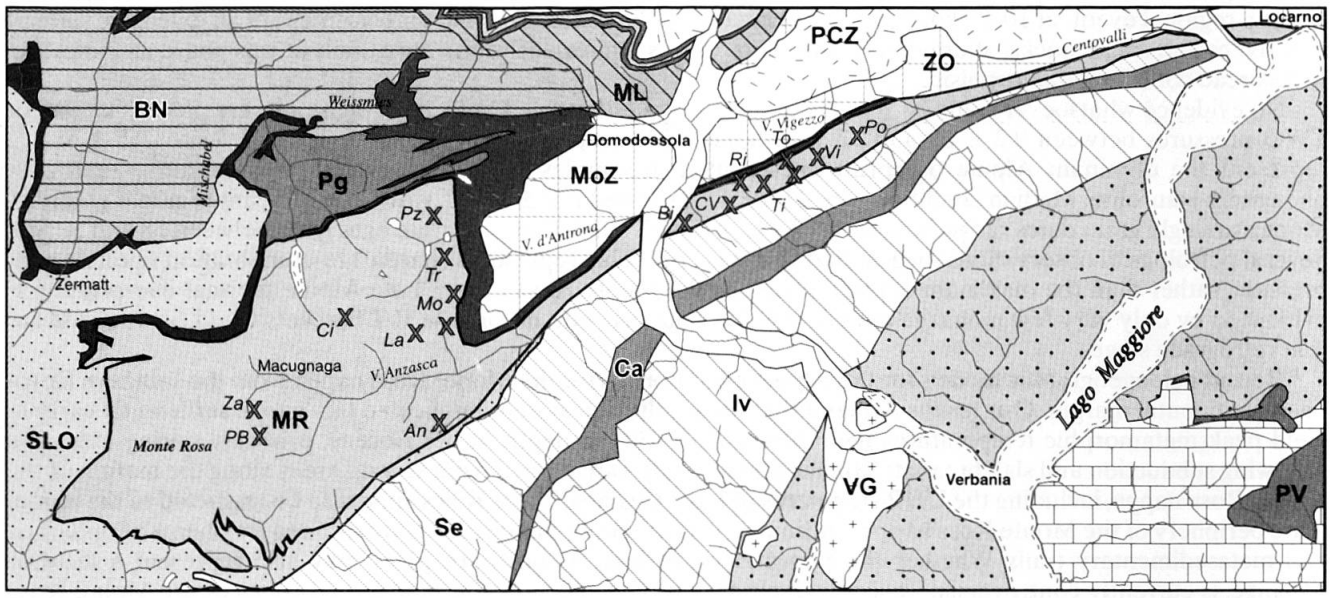

Fig. 1 Tectonic overview of the Monte Rosa (MR) nappe, with major tectonic units from the Tectonic Map of Switzerland (SPICHER, 1980). BN = Bernhard nappe, SLO = Schistes lustrés – Ophiolite zone, Ca = Canavese zone, Iv = Ivrea zone, MoZ = Moncucco zone, ML = Monte Leone nappe, PCZ = Pioda di Crana zone, Pg = Portjengrat unit, PV = Permian volcanics, Se = Sesia Zone, VG = late Variscan granites, ZO = Zone of Orselina. Sample locations shown by X.

temporal evolution of the Monte Rosa nappe (BEARTH, 1952; CHOPIN and MONIÉ, 1984; DAL PIAZ and LOMBARDO, 1986; FREY et al., 1976; HUNZIKER, 1970; HUNZIKER and BEARTH, 1969; HUNZIKER et al., 1992; HUNZIKER and MARTINOTTI, 1984; KÖPPEL and GRÜNENFELDER, 1975; MONIÉ, 1985; ROMER et al., 1996; RUBATTO AND GEBAUER, 1999) indicated Alpine, Variscan, and older ages. Substantial disagreement remains regarding the significance of many of the metamorphic ages in these studies and the discrepancies between dates obtained (e.g. PAQUETTE et al., 1989). The difficulty of interpretation is partly due to problems with specific isotopic systems used (such as excess argon, partial thermal resetting), but a major shortcoming has to do with the selection and documentation of mineral phases used to date the samples. Unfortunately, the loss of structural context incurred when separating mineral fractions from polymetamorphic samples renders a reliable integration of petrologic information impossible. Particularly controversial are age data indicating metamorphism in the Cretaceous, based on Rb–Sr and Ar–Ar dating (CHOPIN and MONIÉ, 1984; HUNZIKER, 1970; MONIÉ, 1985) obtained on samples from peripheral parts of the Monte Rosa nappe, including the Furgg Zone and the Gornergrat Zone. For the latter, recent results by RUBATTO and GEBAUER (1999), who made use of the high spatial resolution of the ion microprobe (SHRIMP) to date multiphase zircons from a metaquartzite, indicated a long sequence of events (from ~700 to 34 Ma), but with no indication of activity leading to zircon growth in the Cretaceous. These authors concluded that the most external zircon zones, dated at 35 Ma, correspond to high pressure conditions for the metaquartzite, estimated at $P < 14$–15 kbar and $T < 550$ °C. It is difficult, however, to ascribe the dates obtained on a few individual rims of zircon grains to a specific petrogenetic stage of the metamorphic evolution of their host rock. In addition, the regional significance of these data in not clear, since MASSON et al. (2000) have voiced doubt whether the Gornergrat slice belongs to the Monte Rosa nappe (see also DAL PIAZ, 2001). For the main part of the latter, no corresponding age dates are available, but it is worth noting that high-pressure garnet from Dora Maira gave a Lu–Hf age of 32.8 ± 1.2 Ma (DUCHÊNE et al.,1997).

Granitoid rocks predominate the Monte Rosa nappe. A pioneering study by FREY et al. (1976) combined petrology, oxygen isotope thermometry, and geochronology to investigate granitic samples. While substantiating the complex polyorogenic history, with Variscan and Alpine parts, the results of that study lacked in resolution to document the evolution in detail, both with respect to the temporal and metamorphic conditions. CHOPIN and MONIÉ (1984) and DAL PIAZ and LOMBARDO (1986) added quantitative detail to the Alpine metamorphic high-pressure conditions by studying, respectively, pelitic and mafic samples. However, both of these studies obtained their samples from mélange zones near the margin or roof of the Monte Rosa nappe, and it is not clear when and how these fragments became incorporated in the main mass of the thrust sheet.

To overcome some of the limitations of granitic samples, the present investigation put its focus on pelitic schists and subpelitic paragneisses. These make up a good part of the pre-Variscan basement complex and occur, more sparsely, within the large granitoid masses as well (BEARTH, 1952; DAL PIAZ, 2001). We report on pelitic samples collected from central and eastern parts of the Monte Rosa nappe, where paragneiss units had been mapped notably by MATTIROLO et al. (1913), BEARTH (1952), and REINHARDT (1966).

Following an account of the geological setting and previous results, we present microstructural and petrologic evidence used to constrain the metamorphic evolution of our metapelite samples. Wherever possible, we obtained thermobarometric results for the same samples, from which single grains of monazite had been selected and separated from thin section, using a set of consistent selection criteria. Chemical Th–U–Pb dates and isotopic Th–Pb ages (obtained using laser ablation PIMMS) for these monazite grains are presented (SCHERRER et al., 2001a). Because our approach utilizes the full context information about the grains we dated, and because monazite has such a high closure temperature for Pb-diffusion (PARRISH, 1990), the results obtained afford a reliable interpretation of several stages of the metamorphic evolution. Implications are addressed in two chapters, first in terms of the polymetamorphism of pelites and the behaviour of monazite in these, and then in terms of the evolution of the Monte Rosa nappe as a whole. Finally, the significance of this nappe in the Alpine collision belt, its emplacement and the exhumation of high-pressure rocks are discussed.

2. Geological framework

Figure 1 shows the Monte Rosa nappe in its present tectonic context, at the same level as the Gran Paradiso nappe of the Western Alps (DAL PIAZ and LOMBARDO, 1995) and the Adula nappe of the Central Alps further east (PFIFFNER and TROMMSDORFF, 1998). The Monte Rosa nappe is

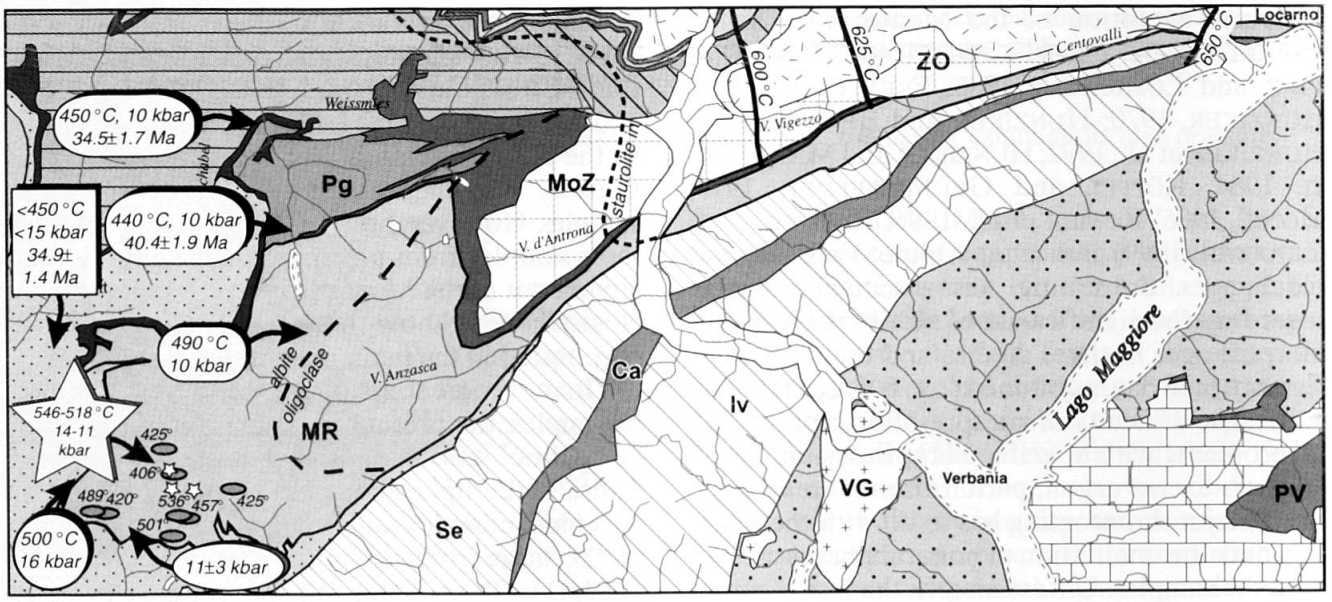

Fig. 2 Metamorphic conditions compiled for the Monte Rosa nappe. Note two distinct stages of evolution:

1. Thermobarometric data in boxes refer to conditions of early Alpine high-pressure (eclogite) stage. Data symbols: For *eclogites*: oval – DAL PIAZ and LOMBARDO (1986); star – BORGHI et al. (1996); for *metagranites*: oval – FREY et al. (1976); for metapelite: circle – CHOPIN and MONIÉ (1984); for *phengite-quartzite*: rectangle – RUBATTO and GEBAUER (1999).

2. Mineral zone boundaries and isotherms (600, 625, 650 °C) characterize Barrovian overprint (the "meso-Alpine" stage of HUNZIKER et al., 1992), the thermal structure of which crosscuts major tectonic boundaries. Albite-oligoclase isograd from BEARTH (1958), staurolite zone boundary from NIGGLI (1970), Barrovian isotherms from TODD and ENGI (1997). For tectonic units refer to Fig. 1.

immediately rimmed by several Pennine thrust sheets comprising Mesozoic ophiolites and metasediments, and showing abundant evidence of high-pressure Alpine metamorphism. The pre-Variscan metamorphic basement of the Monte Rosa unit is of sillimanite-Kspar-grade, includes migmatites and was intruded by massive granites (initial $^{87}Sr/^{86}Sr$: 0.712) and granodiorites during the late Paleozoic, as interpreted by HUNZIKER (1970; Rb–Sr isochron: 310 ± 50 Ma), KÖPPEL and GRÜNENFELDER (1975; U–Pb monazite: 260 ± 5 Ma) and recently confirmed by LANGE et al. (2000; U–Pb data on magmatic zircon and monazite) and LIATI et al. (2001; U–Pb SHRIMP data on zircon: 272 ± 4 Ma). Deformed Monte Rosa granite dated by HUNZIKER (1970; Rb–Sr isochron: 260 ± 10 Ma, initial $^{87}Sr/^{86}Sr$: 0.713) and ages near 250 Ma obtained on the regionally widespread foliation-forming white micas (HUNZIKER and BEARTH, 1969) lead these authors to propose a late-Variscan (Permian) metamorphic event. Its character remains ill constrained (FREY et al., 1976; HUNZIKER et al., 1992) but it seems to correlate in time with magmatic activity that produced both granitic stocks and dykes (aplites and pegmatites), but no mafic dykes. Changes produced during the Alpine orogenic cycle differ in intensity, leaving relics in many areas and rock types. The overprint is strongest near shear zones, in peripheral part ("Schieferhülle"; BEARTH, 1952) of the Monte Rosa granite, and in the easternmost section of the nappe, i.e. the Southern Steep Belt between Valle d'Ossola and Locarno. While in the latter area an amphibolite facies overprint effaced most of the high-pressure characteristics of the earlier Alpine metamorphism, this overprint diminishes in intensity and pervasiveness towards the West. Low-temperature eclogite facies relics thus occur far more frequently to the West of Valle d'Ossola, despite the regionally characteristic postkinematic albitization (BEARTH, 1952) that may be linked to late Alpine hydrothermal activity (PETTKE et al., 1999). Notably, in the abundantly undeformed portions of Monte Rosa granite, no evidence has been reported of the high-pressure breakdown of plagioclase to sodic pyroxene + zoisite + quartz, which is a widespread assemblage in the adjacent Sesia-Lanzo zone (e.g. Monte Mucrone; COMPAGNONI and MAFFEO, 1973; OBERHÄNSLI et al., 1985). As outlined above, the age of Alpine high-pressure conditions in the Monte Rosa nappe is still being debated (mid-Cretaceous or Eo-/Oligocene?), whereas the age of the later thermal overprint is constrained to 34–28 Ma (KÖPPEL et al., 1981; ROMER et al., 1996; PETTKE et al., 1999). Looking at the polymetamorphic history of the entire nappe in some more detail, a number of limits in

the present state of understanding emerge, to which the present study may contribute:

– Peak metamorphic conditions reached during the pre-Variscan evolution are not quantitatively known. However, assemblages and local textures were meticulously documented by (BEARTH, 1952) and show the following reaction sequence to be regionally widespread in metapelites: Cordierite first formed at the expense of biotite and was then pseudomorphosed by sillimanite; garnet + sillimanite + biotite occur as a restite assemblage veined by quartz-feldspar-metatectites; K-feldspar is abundant, with much of the muscovite (and sericite) appearing texturally late. Jointly, these observations indicate partial melting under upper amphibolite facies conditions at medium to low pressures. The absence of andalusite and orthopyroxene, as well as the sparsity of kyanite indicate temperatures near 700 °C and pressures of 3–6 kbar. No regional metamorphic gradients have been documented for this pre-Variscan stage. While early studies ascribed kyanite to a late (but pre-granitic!) stage, subsequent workers (DAL PIAZ, 1971; DAL PIAZ and LOMBARDO, 1986) reinterpreted kyanite to be part of early Alpine assemblages.

– The Permian metamorphism is even less well constrained, presumably because it reached conditions of a lower grade than both the earlier metamorphism and the subsequent Alpine high-pressure stage. In granitoids regionally widespread assemblages include oligoclase, orthoclase, and $2M_1$ muscovite (in contrast to to Alpine HP-assemblages with microcline, ($2M_1$ or 3T) phengite plus either oligoclase or albite + epidote); oxygen isotope temperatures for muscovite indicate temperatures between 520 and 560 °C (FREY et al., 1976). Pressures estimated in that same study are given as 2–4 kbar, but the precise basis is not clear. No studies of mafic or pelitic rocks have been conducted so far to derive pressure conditions for the Permian metamorphism or to document the spatial variability of its intensity and character, hence possible tectonic implications remain mysterious. Temporally, the relation between Variscan magmatism and the Permian metamorphic overprint is certainly close. Spatially, the situation is not so clear, since no discrete thermal aureoles have been recognized away from the intrusive contacts (e.g. in the W and SW parts of the nappe), though these are undisturbed in several areas (BEARTH, 1952). (We interpret the high grade gneiss schollen described in that study from within undeformed portions of the Monte Rosa granite as fragments of the pre-Variscan metamorphic basement.) Evenso, it seems entirely possible that the Permian event essentially represents contact metamorphism, i.e. that heating was due mostly to acid magmatism rather than crustal thinning.

– The early Alpine phase, apart from the age uncertainty mentioned, is fairly well established as a high pressure overprint. Evenso, the number of samples documented by modern methods is quite limited: FREY et al. (1976) derived oxygen isotope temperatures of 440–490 °C from five phengite samples of Monte Rosa metagranite. Using this range and the compositions of phengite (3.3–3.4 Si per formula unit) reported in that same study, the calibration by MASSONNE and SCHREYER (1987) indicates maximum pressures of 9–10 kbar. A similar range, bracketed between 9 ± 1 and <14 kbar was delimited from low-temperature eclogites by DAL PIAZ and LOMBARDO (1986), with temperatures between 402 and 536 °C based on garnet-clinopyroxene thermometry. (Note that these temperatures were obtained using the calibration by ELLIS and GREEN (1979). The more recent version by KROGH (1988) yields 337–488 °C.) For three garnet mica schists studied by BORGHI et al. (1996), thermobarometry gave 515–545 °C and 11–14 kbar for what these authors identified to be "first generation assemblages" on textural grounds, but with no mineral age data available. On the basis of three samples from each of the Internal Pennine "Massifs" (Monte Rosa, Gran Paradiso, and Dora Maira), these authors also inferred a PT-path for the Alpine HP-evolution, supposed to be valid for all of the units. The regional distribution of all of the PT-data available so far for this stage is shown in figure 2. It would be hazardous to infer a metamorphic field gradient from these data, owing to likely systematic differences between the methods used and the possibility of partial re-equilibration following emplacement. Higher pressures, at temperatures near 500 °C, have been reported from peripheral parts in the SW of the Monte Rosa nappe. Thus, CHOPIN and MONIÉ (1984) obtained 16 kbar from an unusual metapelite sample, and LE BAYON et al. (2001) derived pressures as high as 23 kbar from whiteschists (see PAWLIG and BAUMGARTNER, 2001); the latter conditions are said to reflect the peak of Alpine eclogite facies metamorphism in that area.

– Conditions for this ("meso-") Alpine lower-pressure overprint reached only greenschist facies in the western portion of the Monte Rosa nappe, with a well defined albite-oligoclase isograd (BEARTH, 1958) and, some kilometers further to the NE, the staurolite zone boundary (DAL PIAZ, 1971; NIGGLI, 1970) indicating a field gradient (Fig. 2) that mimics the pattern of regional isotherms for the Central Alps (TODD and

Tab. 1 Metapelite samples from the Monte Rosa nappe studied. Coordinates refer to Swiss topographic maps; mineral abbreviations according to KRETZ (1983).

Sample	X-Coord.	Y-Coord.	Alt.(m)	Sample location	Rocktype	Major mineral constituents	Minor	Accessories
An9901	649'850	87'200	2095	W of P. Tignaga, just E of small lake	Grt-bearing mica gneiss	Qtz, Bt, Ms, Grt, Chl	Tur	Ilm, Rt, Mnz
Bi9801	667'200	102'600	640	Alpe Bisoggio, SE Beura	Grt±St-Bt-Ms gneiss	Grt, St, Bt, Ms, Chl, Qtz, Kfs, Pl,		Ilm, Tu, Mnz
Bi9802	667'200	102'600	640	Alpe Bisoggio, SE Beura	Grt±St-Bt gneiss	Grt, ± St, Bt, Ms, Chl, Qtz, Kfs, Pl		Ilm, Tu, Mnz, Zrn
Ci9901	644'500	97'050	2920	between Ofentalpass and P. Cingino Sud	Grt-bearing Ms gneiss			
CV9801	670'400	103'050	1785	NE A. Corte Vecchia	Grt±St-Bt gneiss			
La9901	648'300	94'550	2645		Grt-Bt-Ms schist			
La9903	649'900	95'650	2690	Just SW of Pt 2713 along Cresta di Lareccio	Grt-Bt-Ms schist			
La9904	649'900	95'650	2690	Just SW of Pt 2713 along Cresta di Lareccio	Grt-Bt-Ms schist			
La9905	650'025	95'600	2635	block within few meters of original position	Grt-bearing Ms gneiss			
La9906	650'350	95'700	2620	SE of P. San Martino on S face of SW ridge off Pt. 2733	Grt-bearing mica gneiss			
La9907	647'900	94'750	2785	between P. Lame and Passo delle Lonze along ridge	Grt-Bt-Ms schist			
La9908	647'800	94'700	2707	Psso delle Lonze	Grt-Bt-Ms schist			
Mo9801	652'250	97'600	2385	W Pso. del Mottone	Grt-bearing mica gneiss	Grt, Qtz, Ms, Bt, Chl, Ilm, Plag, K-feld,	Aln	Rt, Mnz
Mo9802	652'250	97'600	2385	W Pso. del Mottone	Grt-bearing mica gneiss	Grt, Qtz, Ms, Chl, Plag, K-feld, Ilm, Rt, Bt	Hem	Mnz, Aln
Mo9803	651'000	95'950	2265	E P. San Martino	Grt-bearing mica gneiss	Ms, Qtz, Bt, Grt, Ap,		
Mo9804	651'050	95'950	2120	E P. San Martino	Grt-bearing mica gneiss	Qtz, Bt, Ms, Chl, Grt, Kfs,		Ilm, Rt, Mnz
PB9901	638'850	87'750	3175	Just below Pt 3180 (NW) on Pizzo Bianco	Grt±St-Bt gneiss			
PB9902	638'850	87'750	3175	Just below Pt 3180 (NW) on Pizzo Bianco	Grt±St-Bt gneiss			
PB9904	638'350	88'400	2610	Just SE of Pta C. Battisti on N side of Locciechiuse	Grt±St-Bt gneiss			
Pi9701	670'900	104'800	1860	NW Pta I Pisoui, along steep trail just below peak	Grt-Bt-Ms schist	Qtz, Plag, Ms, Bt, Grt1, Grt2, Ilm, Ap		Zr, Mz, Rt, Aln
Po9701	678'300	105'950	1750	NE La Porcella	Grt-St-Bt-Ms schist			
Po9702	678'300	105'950	1750	NE La Porcella	Grt-St-Bt-Ms schist			
Po9703	678'300	105'950	1750	NE La Porcella	Grt-St-Bt-Ms schist	Qtz, Grt, Bt, Ms, St		Mnz, Zr
Pz9702	650'350	100'750	1080	NE L. di Antrona	Grt-bearing Sil-Bt gneiss			
Pz9703	651'250	103'200	1940	E of Forcola	Grt-bearing Sil-Bt gneiss			
Pz9704	651'250	103'200	1940	E of Forcola	Grt-bearing Sil-Bt gneiss			
Pz9905	649'325	103'075	2490	N of Cime di Pozzuoli (Pt 2602) on ridge to N.	Grt±St-Bt gneiss			
Pz9906	649'325	103'075	2490	N of Cime di Pozzuoli (Pt 2602) on ridge to N.	Grt±St-Bt gneiss			
Pz9907	650'200	100'350	1080	SW of Lago di Antrona along trail	Grt±St-Bt gneiss			
Ra9701	675'600	105'550	2200	S side P. Ragno-Nona	Grt-St-Bt-Ms schist			
Ra9703	675'250	105'050	2200	S P. Nona, W Costa Nera	Grt-Hbl-Bt schist			
Ri9801	670'600	104'300	1450	NW A. Rina	Grt±St-Bt gneiss	Bt, Ms, Chl, Grt, Qtz, Kfs, Ilm		Ap, Tur, Mnz
Ri9802	670'600	104'300	1450	NW A. Rina	Grt±St-Bt gneiss	Qtz, Kfs, Chl, Ms, Bt, Chl, Grt, Pl	St, Ap	Ilm, Mnz, Aln
Ti9701	672'125	103'900	2110	S P. Tignolino	Grt-Bt-Ms schist			
Ti9801	671'300	103'550	1740	SW P. Tignolino	Grt±St-Bt gneiss	Qtz, Ms, Chl, Grt, St, Ilm	Bt	Zr, Mz, Aln
To9801	673'750	105'650	1895	NE of M. Togano, S of P. Marcio	Grt-Tur-Bt-Ms schist	Qtz, Bt, Ms, Tur, Grt, Ilm, Plag	Hem	Zr, Mz
To9802	673'850	104'550	2190	S of M. Togano	Grt±St-Ms gneiss	Qtz, Ms, Ilm, Grt, St, Chl, Plag		Zr, Mz
Tr9902	651'000	99'050	1800	east of A. Larticcio where trail crosses main creek gully	Grt-Bt-Ms schist	Qtz, Ms, Bt, Grt, Ap	Ilm, Chl	Rt, Mnz
Tr9903	651'800	98'800	2247	Point 2247 N of Psso di Trivera, SW of Punta di Trivera	Grt-Bt-Ms schist			
Tr9904	651'900	98'150	2300	just to the NE of Psso di Trivera	Grt-bearing mica gneiss			
Vi9702	674'220	104'900	2195	SE M. Togano	Grt-bearing mica schist	Grt, ±St, Bt, Ms, Pl, Qtz, Chl	Aln, Ilm, Tur	Xen, Zrn, Rt, Mnz
Za9701	637'500	89'300	2140	E A. Pedriola, block (of local origin)	Ky-bearing Grt-Ms schist	Grt, Cld, Qtz		Mnz
Za9702	637'300	89'450	2070	E A. Pedriola	Grt-bearing Sil-Bt gneiss	Sil, Phe, Qtz, Grt(1+2)		Mnz
Za9703	637'350	89'675	2045	NE A. Pedriola, block (of local origin)	Ky-bearing Grt-mica schist	Sil, St? Phe–> Bt	Rt, Ilm, Chl, Pl	
Za9705	637'900	89'900	2070	NE A. Pedriola, block (of local origin)	Ky-bearing Grt-mica schist			

ENGI, 1997). Only for this last overprint is it clear that P-T-conditions within the Monte Rosa nappe are comparable to those of neighbouring tectonic units; for the early Alpine and previous phases of the polymetamorphic evolutions, this has not been established and indeed appears unlikely to be the case. The age and duration of that last Alpine thermal overprint are difficult to delimit precisely. A decreased in intensity and age from East to West is probable, but the time interval over which mineral transformations took place probable increased in the same direction. This pattern is indicated by available isotopic and fission track ages (discussed by ZINGG and HUNZIKER, 1990, HUNZIKER, 1992, and ROMER et al., 1996), and such a pattern is also expected on the basis of thermal models (ENGI et al., 2001; ROSELLE et al., 2002) for the thermal relaxation following peak regional metamorphism.

Paleogeographic reconstructions for the Monte Rosa nappe have come to widely differing conclusions, with some authors attributing the slice of continental crust to paleo-Africa, to the Briançonnais, or to the European margin. Though the debate is ongoing, recent suggestions (FROITZHEIM, 2001; DAL PIAZ, 2001) favor the latter scheme, based on the high pressure metamorphism (FROITZHEIM, 1997; GEBAUER, 1999; RUBATTO and GEBAUER, 1999) having reached its maximum depth on subduction during Eo- to Oligocene times.

3. Selection and analysis of single grain monazite

Samples collected for the present study are listed in table 1, which also gives summary of minerals observed. Monazite grains occur in most of the paragneiss samples of the Monte Rosa nappe, but their abundance, size, and structural context are quite variable (SCHERRER et al., 2001a).

The microscopic context, e.g. monazite inclusions in garnet *versus* single monazite grains or clusters within the matrix, permits a clear separation of two phases of monazite growth in the metapelites. Well shielded monazite inclusions in garnet are compositionally homogeneous and range in size from <10 μm to >100 μm. In pelites and subpelites, such inclusions are found in large garnet porphyroblasts. A texturally different type of monazite inclusions, displaying symplectic textures (SCHERRER et al., 2001a) occurs as well, and these have been attributed to rapid decompression following high pressure conditions during Eo- to Oligocene times (SCHERRER et al., 2001b). Far more abundant than either of these types are monazite grains in the matrix, occurring either at grain boundaries or, quite commonly, within biotite, white mica, or one of the aluminosilicate phases. These matrix monazites display many different morphologies, from fine grained trails or single grains to porphyroblastic relics. Texturally, they commonly appear partially recrystallized in between matrix minerals or fully recrystallized with these.

For the purpose of dating specific stages of the polymetamorphic evolution, we selected samples with sufficiently large monazite grains (>50 μm if possible) from texturally interpretable contexts, i.e. inclusions in garnet porphyroblasts, equilibrated metamorphic assemblages within the matrix, or reaction textures attributable to a specific breakdown reaction. The approach used in this study for Th–U–Pb dating of monazite is described by SCHERRER et al. (2000, 2001a). A combination of techniques was applied to document microstructures and select grains for dating. Besides the petrographic microscope, SEM and electron microprobe images (BSE and X-ray maps) proved most useful. The selection criteria required by the geochronological methods available set limits on what types of monazite could be dated and did not allow, for example, the analysis of certain fine grained reaction products, such as symplectitic monazite. Where the size and homogeneity of grains were sufficient, single monazite grains were first analyzed by electron microprobe and then painstakingly extracted from specially prepared thin sections, using techniques detailed by SCHERRER et al. (2000). Drilled out monazite grains were then analyzed (SCHERRER et al., 2001a) by XRF microprobe (at University of Bern) to obtain chemical Th–U–Pb ages, and a subset of the samples was subsequently dated by PIMMS (laser-ablation Plasma-Ionisation Multi-collector Mass Spectrometry, at NIGL, British Geological Survey).

Chemical and isotopic age data obtained from monazite grains extracted from our metapelite samples of the Monte Rosa nappe (Tab. 1) fall into three classes: Chemically homogeneous monazite inclusions in large garnet porphyroblasts are of Permian origin (Fig. 3a, b). Matrix monazite generally indicate Alpine ages (Fig. 3c, d), or they have a Permian core surrounded by an Alpine rim. Heterogeneous grains, some with clear core-rim structures and others with complex resorption features, seem to be more common to the west of the Antrona ophiolite and rare in the easternmost part of the nappe, i.e. the Southern Steep Belt. Monazite of Permian age only was observed in one sample, which apparently has escaped the effects of Alpine metamorphism.

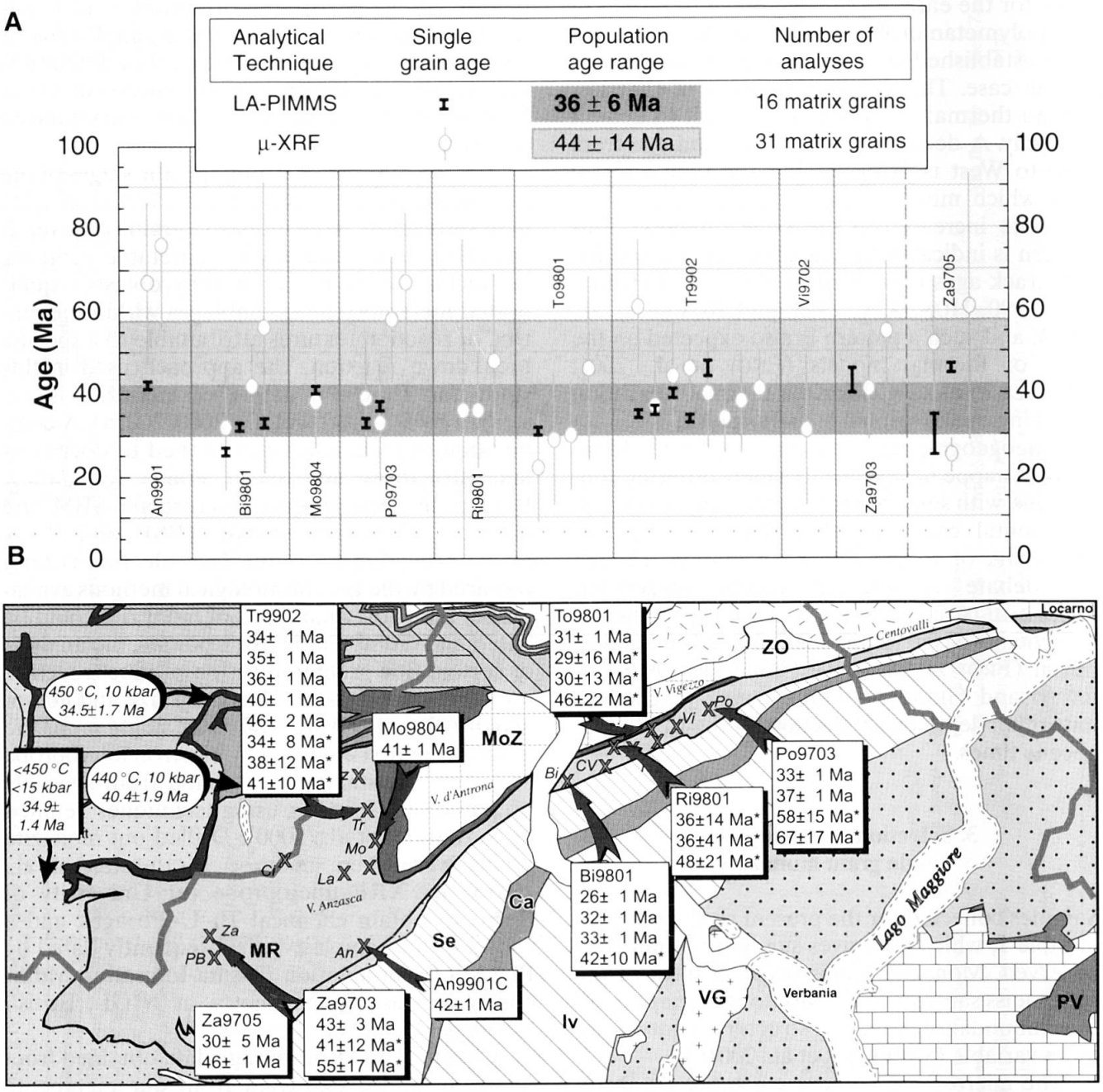

Fig. 3 Age data for single monazite grains obtained by chemical and isotopic dating methods applied to the same grains. μ-XRF data denoted by asterisks; all others are LA-PIMMS data (SCHERRER et al., 2001a).
(A) Data for Permian monazite population: 9 inclusions in garnet, 3 zoned matrix grains with inherited cores, 10 pre-Alpine matrix grains; (B) regional distribution of Permian ages. Data in brackets refer to cores of monazite grains from the matrix; all other grains were included in garnet porphyroblasts. 2σ-error on PIMMS data is smaller than symbol size; uncertainty given for population of electron microprobe ages is nominal scatter, ignoring the error of individual EMP ages (60–100 Ma).

Details of the age distribution in each sample are discussed in the subsequent chapter, in the context of the local textures and metamorphic assemblages to which the dated monazite grains belong. In the following, age results shown are those with the lowest analytical uncertainty available for any monazite grain. Errors (SCHERRER et al., 2001a) are quoted in the text at the 2σ-level and, to identify the technique used, chemical XRF-dates are identified by an asterisk (e.g. 260 ± 25 Ma*), whereas PIMMS-ages are shown without a symbol (e.g. 325 ± 8 Ma).

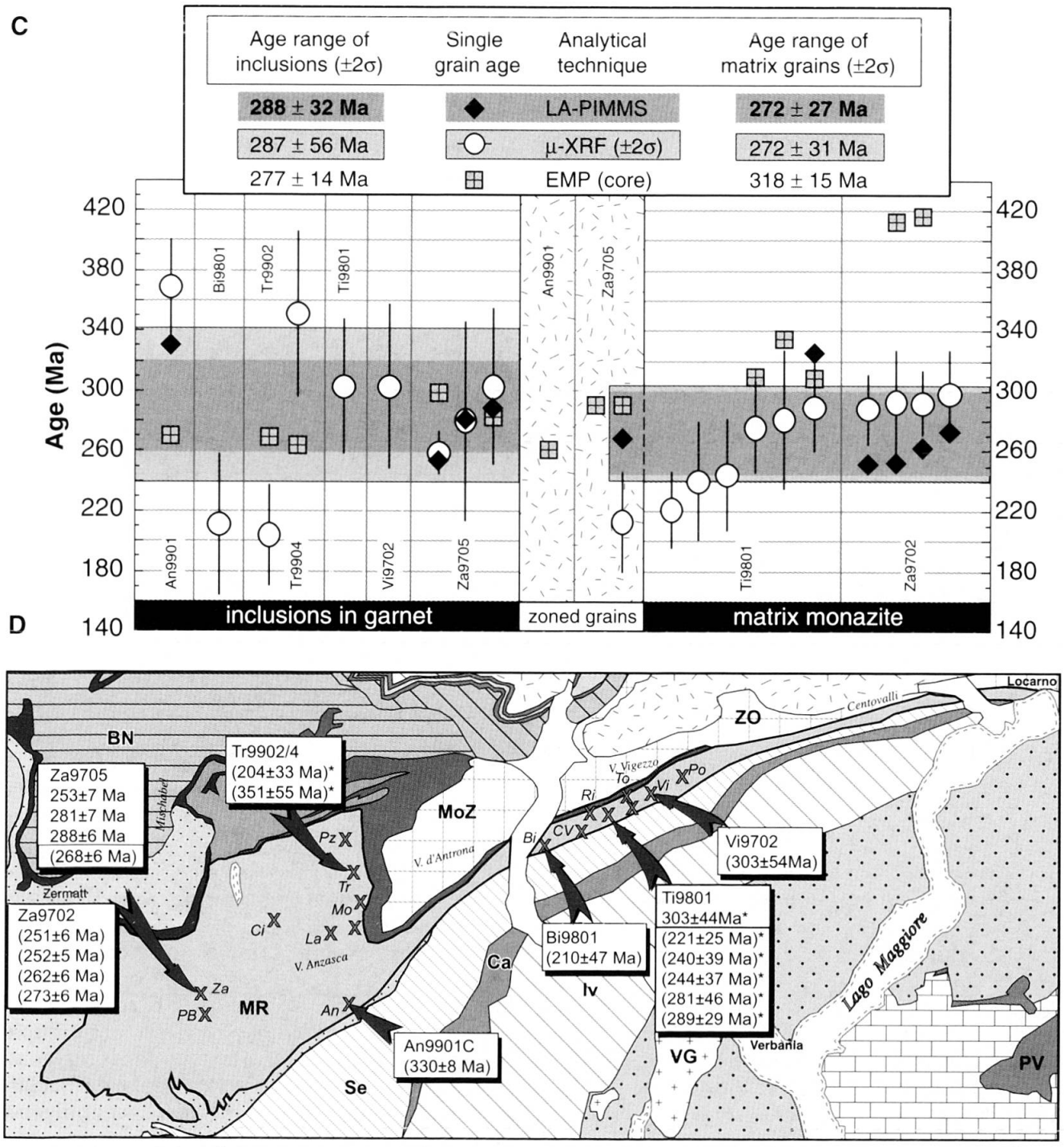

Fig. 3 (cont.) (C) Alpine monazite population: all 36 grains from matrix; (D) regional distribution of Alpine ages. Data in westernmost box from RUBATTO and GEBAUER (1999) for ophiolitic units adjacent to Monte Rosa nappe; data in oval boxes from FREY et al. (1976) for Monte Rosa metagranites.

4. Petrologic evolution

4.1. PETROGRAPHIC CHARACTERISTICS OF MONTE ROSA METAPELITES

Thorough petrographic investigations of metapelites were previously reported by BEARTH (1952), DAL PIAZ (1963, 1964, 1966, 1971), REINHARDT (1966), WETZEL (1972), and BORGHI et al. (1996). Typical constituents of Monte Rosa paragneisses include quartz, white mica (phengite and/or muscovite), biotite, garnet, ilmenite, rutile, apatite, monazite and zircon, with staurolite, kyanite and/or sillimanite, chlorite, plagioclase (albite or oligoclase), and allanite ocurring in some samples only. Local textural and mineralogical observations indicate that some metapelites retain partial evidence of their polymetamorphic

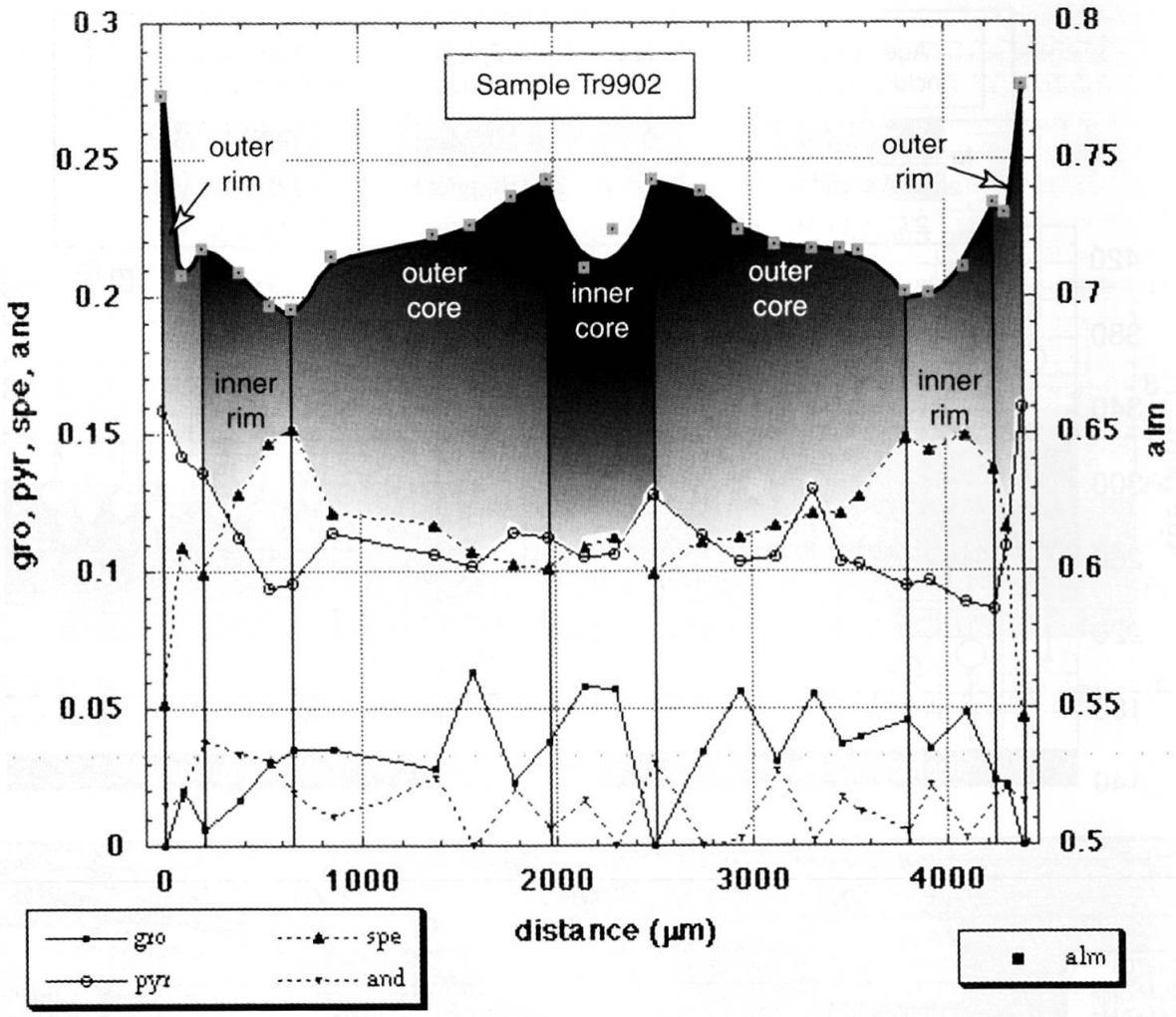

Fig. 4 Compositional profile across large garnet porphyroblast in sample Tr9902, arguably representing three generations of garnet. A monazite inclusion within the core of similar Za9705 garnet indicates a uniform age of 259 ± 14 Ma, whereas large monazite grains in the matrix display a core-rim structure with a Permian core and an Alpine rim.

history, whereas others apparently reset completely at some stage of their evolution. Hence it is essential to characterize assemblages at the grain scale, to check for local mineral (dis)-equilibria and interpret the state of resetting prior to performing thermobarometry or mineral chronometry.

Within most of the samples analysed, garnet is Fe-rich (Alm_{60-85}) and commonly occurs in (at least) two generations and with some grains showing typical prograde zonation or multiple overgrowth profiles (Fig. 4). Staurolite is regionally most abundant east of Val d'Ossola, particularly in the Southern Steep Belt, where generally few

Tab. 2 Single crystal monazite ages (Tab. 1) and multi-equilibrium thermobarometry (TWQ) for metapelites from the Monte Rosa nappe.

Sample	Bi9801a	Mo9801c	Pb9901c	Ri9801b2	Ri9801c4	Po9703b	Pz9905b
# rxn	3	3	3	4	3	3	3
P (kbar)	11.0 ± 1.0	11.7 ± 1.3	9-12	12.1 ± 1.6	12.0 ± 1.5	10.0 ± 1.0	9.2 ± 1.8
T (°C)	610 ± 25	755 ± 65	730 ± 30	735 ± 55	730 ± 50	595 ± 25	620 ± 60
P (kbar)			17–21 *				
T (°C)			770 ± 30 *				
Age range (Ma)	33 ± 1 to 26 ± 1	41 ± 1				37 ± 1 to 33 ± 1	
# grains	3	1				2	

rxn: number of independent equilibria used by TWQ (BERMAN, 1988).
grains: number of matrix grains dated ($^{208}Pb/^{232}Th$).
* relic higher pressure stage (?) indicated by some equilibria.

relics of high pressure metamorphism have been reported for the Monte Rosa nappe. However, staurolite of an earlier generation is present also in several samples from further West, outside the staurolite zone boundary (NIGGLI and NIGGLI, 1965; NIGGLI, 1970), in samples retaining high pressure assemblages. On the other hand, chloritoid, phengitic mica (3.3–3.4 Si p.f.u.), rutile, plus kyanite or sillimanite, have been found only to the west of the Antrona trough (Fig. 2). Plagioclase is sparse and where analyzed is of oligoclase composition (~An_{30}). Three types of white mica could be distinguished, with paragonitic and phengitic mica being restricted to the western samples, whereas muscovite (<3.1 Si p.f.u.) is widespread throughout the nappe. Where rutile occurs, it is commonly rimmed by ilmenite, except where protected within in porphyroblasts of gar_1 or $stau_1$. Chlorite appears mostly linked to late greenschist facies overprinting, but in some samples it is clearly part of the higher pressure assemblages.

Based on textural relationships, Alpine metamorphic assemblages can be divided into higher and lower pressure assemblages, as previously discussed by BORGHI et al. (1996). At higher pressure the assemblages include Qtz–Ph–Cld–Chl_1–Grt_1–Ky–Rt±Ilm±Pg±St_1 and at lower pressure Qtz–Ms–Bt–Grt_2±St_2±Olig/Ab+Ep.

A select set of individual samples (Tab. 2) and groups thereof are presented below according to petrological criteria and monazite age data.

4.2. METHODS USED

The characterization and interpretation of polymetamorphic samples demands particular attention to microstructural characteristics, such as relics and domains containing neoblasts of one or more phases overgrowing older assemblages. Apart from careful petrography and comparison to suitable petrogenetic grids, the availability of monazite ages from several individual structural domains of a sample has proven most helpful. Assemblages used in this study to constrain metamorphic P-T-conditions were selected *after* monazite grains from the same domain had been age-dated with credible results. The aim was thus to obtain thermobarometric data for a particular stage in the metamorphic evolution of the sample. Of course the simultaneity of monazite growth (or complete recrystallization) and of chemical equilibration of the silicate-oxide assemblage used for P-T-determinations cannot be guaranteed. However, criteria such as the chemical homogeneity of monazite and of the major constituent phases analyzed, their alignment in one and the same penetrative foliation, as well as clean boundaries indicative of textural equilibrium, have been used to support (or reject) the hypothesis. Despite these precautions, the thermobarometric multiequilibrium approach used indicates that we were not always successful in avoiding disequilibrium assemblages. In a few samples, mineral disequilibria were thus detected only when computing phase diagrams based on microprobe data.

All phases of potential equilibrium assemblages, selected from dated samples, were analyzed by electron microprobe (Cameca SX50, 15 kV, 20 nA; WDS mode, using synthetic and natural standards). Analyses were obtained within small domains selected in thin section, where possible on grains in direct contact. Data were screened to ensure sufficient quality of analyses used. Probe data were normalized according to the requirements of the thermodynamic analysis, using TWQ (BERMAN, 1991) with the dataset by BERMAN and ARANOVICH (1996). In addition, we adopted the revised phengite model by MASSONNE and SZPURKA (1997), the improved thermodynamic properties for staurolite by NAGEL et al. (2001), and an ideal activity model for Mg-Fe-chlorite. To avoid large uncertainties in activities, we excluded mineral components present in very low concentration, i.e. $X_{component}$ <0.05 (TODD, 1998).

To evaluate the P-T-conditions preserved in any analyzed assemblage we considered all of the (fluid-absent) equilibria computed to be stable anywhere in the P-T-domain [200–1200 °C, 1–20 kbar]. The intersection pattern of all of the stable and metastable branches of these possible equilibria was inspected as a first indication of the suitability of the complete assemblage. Depending on the number of phase components involved, the number of independent equilibria turned out usually between 4 and 2. In the latter case, a unique P-T-intersection results, reflecting merely the paucity of the assemblage, the quality of which then cannot be evaluated using TWQ alone. In such cases, it was sometimes possible to check the quality of the P-T-result by comparing the observed assemblage against a suitable petrogenetic grid and by performing the following experiment: Assume that the activity of TiO_2 and/or Al_2SiO_5 equals unity, i.e. that the assemblage was in fact saturated in rutile and/or kyanite (or sillimanite), compute the P-T-diagram again. Then evaluate all of the additional equilibria generated as *limiting* the space for which $a(TiO_2)$ <1 and/or $a(Al_2SiO_5)$ <1. This approach thus utilizes not only the phases present, but also includes the observed absence of the respective titanium or aluminosilicate phase(s). Judging by

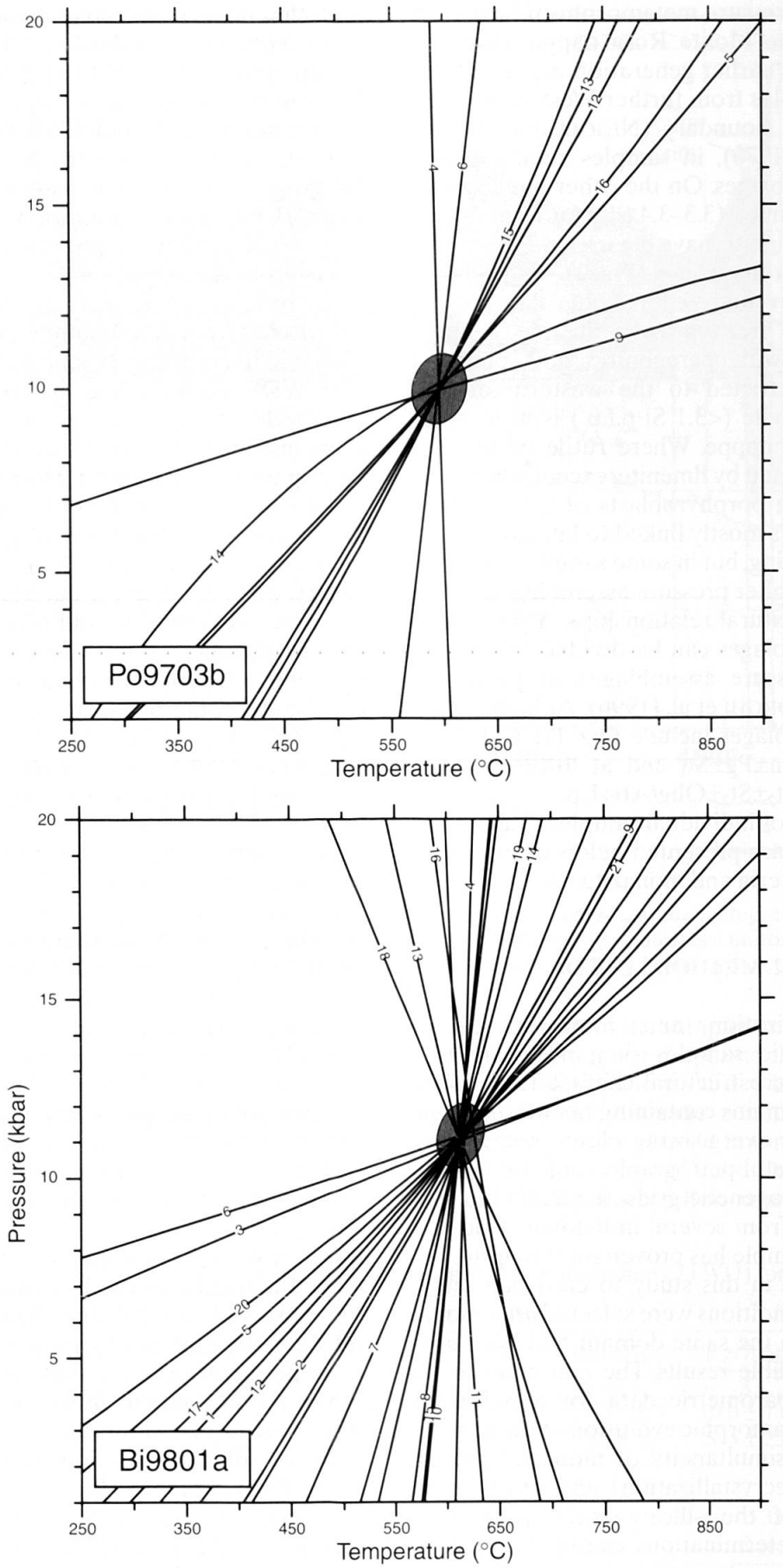

Fig. 5 P-T-diagram showing location of fluid-absent equilibria computed using TWQ for phase compositions measured in samples Po9703 and Bi9801. P-T-uncertainty shown by ellipse. Thermodynamic models used and restrictions applied are discussed in text. Individual equilibria are numbered, for reactions see Appendix.

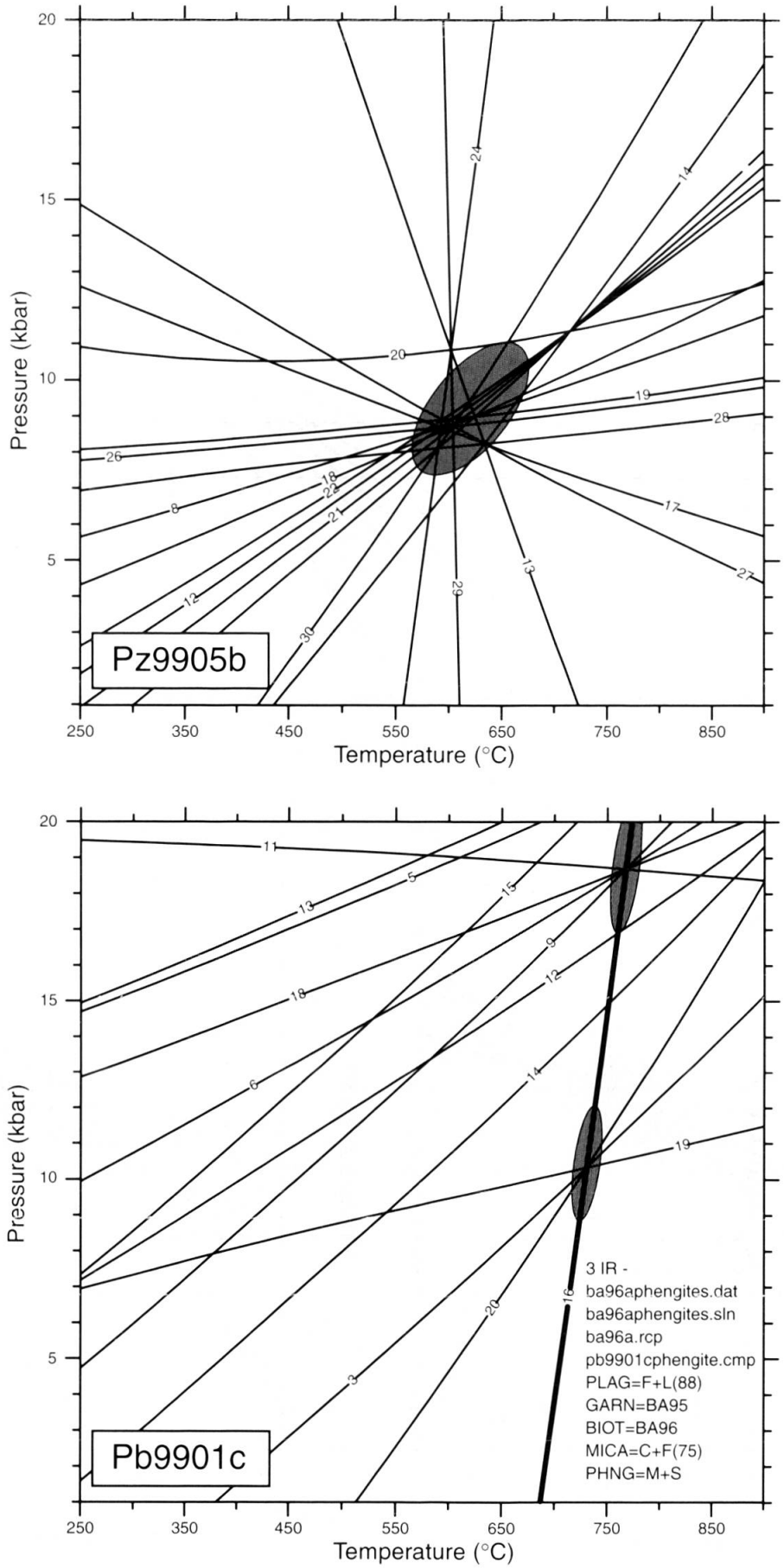

Fig. 6 P-T-diagram showing location of fluid-absent equilibria computed using TWQ for phase compositions measured in samples Pz9905 and Pb9901c. See text and Fig. 5 for further details.

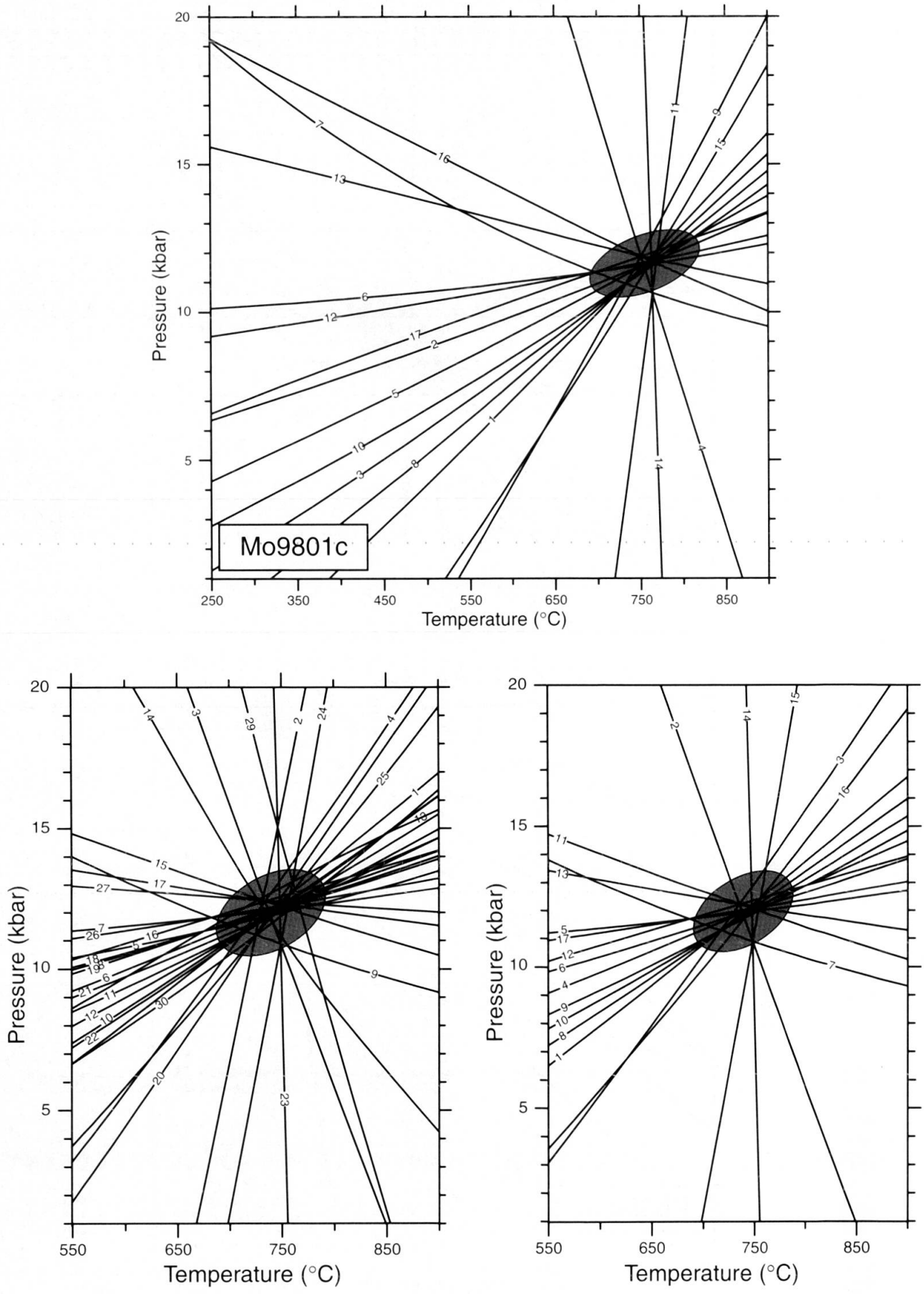

Fig. 7 P-T-diagram showing location of fluid-absent equilibria computed using TWQ for phase compositions measured in samples Mo9801 and in two domains of sample Ri9801. See text and Fig. 5 for further explanations.

the consistency of P-T-intersections and the narrow P-T-fields obtained using this approach, we conclude that many of the metapelites investigated appear to be only very slightly undersaturated in the respective phases. In such cases, this experiment sets very useful additional limits in thermobarometry. Its application is, of course, not restricted to "poor" assemblages, i.e. with only two independent reactions.

Where 3 or 4 equilibria were independent, the dispersion of invariant points in P-T-space was inspected and, in some cases, overall equilibrium appeared to be well preserved (e.g. Figs 5, 7). In other cases, all but a few equilibria seemed well behaved, and outliers involved one particular phase component (Fig. 6). This was commonly found to be siderophyllite or rutile. In the former case, the discrepant results may well be caused by an inadequacy in the thermodynamic model, whereas for rutile petrographic evidence usually indicated an irreversible reaction, such as partial replacement by ilmenite. In either case, the hypothesis of a completely intact equilibrium assemblage could not be maintained, the violating mineral species or component was eliminated, and TWQ analysis continued without it. Results shown in the subsequent paragraphs indicate that completely convincing equilibrium assemblages are indeed rather rare in the samples we investigated, but reliable thermobarometric constraints can be derived from a few of them.

4.3. PERMIAN METAMORPHISM

In several areas, including the central portion of the nappe to the West of Macugnaga, BEARTH (1952) had mapped metasediments showing little or no Alpine overprint. A suite of metapelites, sandwiched between the main mass of Macugnaga augengneiss and granitic tectonites of the Stelli zone, was sampled near Alpe Pedriola, NW of Pizzo Bianco. Most of these samples (Za-suite in Tabs 1 and 2; cf. Fig. 1) show the early stages well preserved. In particular, Za9702 displays no signs of a high pressure or retrograde greenschist facies overprint, i.e. the sample appears to have largely escaped Alpine metamorphism. In contrast to samples of chloritoid bearing garnet-mica gneisses (Za9703, Za9705) from the same area, Za9702 also lacks a penetrative foliation. It contains exceptionally abundant fibrolite and K-feldspar, three generations of garnet, and unusual textural characteristics of biotite and white mica. The earliest generation of garnet is present as subidiomorphic grains (~5 mm in diameter), with no evidence of corrosion or overgrowth on them, but with random needles (sillimanite? up to 3 mm in length) crosscutting the grains. Surrounding this earliest generation of garnet is a fine grained felt of fibrolite plus quartz. This sillimanite-rich felt is thickest at opposing ends of garnet porphyroblasts, suggesting the replacement of previous pressure shadows. A dense cluster of roundish garnet grains overgrew the felt and partially replaced it. The only hint at a weak foliation in this sample is given by corroded platelets of coarse biotite that surround the felt rimming the first generation garnet. Biotite is conspicuously reddish-brown, may show delicate symplectic fringes and was replaced, near its margin to fibrolite, by elongate poikilitic garnet containing quartz, K-feldspar, and abundant tiny ilmenite grains as inclusions. These textural and mineralogical features, notably the extreme enrichment in sillimanite, lead us to interpret this sample as a restitic metapelite. In view of the regional homogeneity of the metapelites (BEARTH, 1952), it appears that a significant portion of the leucosome was lost from its pelitic protolith during or following partial melting. Millimeter-size pockets dominated by quartz and K-feldspar, containing some 30% randomly oriented muscovite and biotite, with only traces of sillimanite, may represent seggregates of such leucosome.

Four monazite grains from the matrix of sample Za9702 were dated, yielding a median age of 252 ± 9 Ma (PIMMS data, Tab. 1). These ages are but slightly younger than those obtained from monazite enclosed in garnet in sample Za9705 taken a few hundred meters away, for which 281 ± 16 Ma resulted. These data represent maximum ages for the garnet from which the respective monazite inclusions were extracted, hence no significant age difference between the porphyroblasts and the matrix monazite can be detected. In sample Za9705, however, monazite grains in the matrix indicate that it has been partially reset, probably due to recrystallization of monazite in the matrix. Ages obtained gave a bimodal distribution: Three monazite grains evidently recystallized at Alpine times (30 ± 5, 46 ± 1, 61 ± 32 Ma*[2]); two grains are zoned, one of which gives an intermediate age (145 ± 5 Ma) probably due to overgrowth of a Permian core by an Alpine rim, the other one appears unaffected (268 ± 6 Ma), as does another matrix monazite (290 ± 120[3] Ma). In a third sample of that suite (Za9703), all of the monazites from the matrix show Alpine ages be-

[2] Where no PIMMS-data are available, XRF-data are quoted and denoted by an asterisk.

[3] Large error due to low Th-contents of grain.

tween 43 ± 3 and 55 ± 17 Ma. Evidently this suite of high-grade metapelites experienced unequal amounts of recrystallization in post-Permian times, with some samples showing Alpine chloritoid ± staurolite ± chlorite, but Za9702 does appear remarkably unaffected by Tertiary events.

Even more exceptional is sample Ti9801 from taken just SW of Pizzo Tignolino, some 8 km SE of Domodossola. Despite the strong strain evident in the Southern Steep Belt portion of the Monte Rosa nappe, this staurolite–chlorite–tourmaline bearing garnet–biotite–muscovite schist indicates the preservation of Permian (and possibly older) ages of monazite within garnet porphyroblasts and in the matrix! For the latter, the median age is 260 ± 25 Ma* from XRF chemical dating, whereas one grain dated by PIMMS gave 325 ± 8 Ma; only one monazite inclusion in garnet could be dated, yielding 303 ± 44 Ma*. As in the previous suite, we infer that the Alpine metamorphism, which in this locality reached lower amphibolite facies conditions, did not reset the Permian ages even in the matrix. Yet the silicate assemblage in this case does not look particularly different from those in neighbouring samples, many of which demonstrably did equilibrate during Alpine times (below). We cannot be sure whether the silicate assemblage in Ti9801 does retain the characteristics of the Permian metamorphism. However, since this sample as well as Za9702 discussed above were taken but a few hundred meters away from intrusive contacts to major granitic bodies, it seems likely that the assemblages were formed by Variscan contact metamorphism and not by a Permian regional event. The P-T-conditions of formation or equilibration were not investigated further.

In several other samples (Tr9902, Tr9904, Vi9702) monazite inclusions in garnet indicate Permian ages, but in all of these the matrix assemblages, including monazite, had evidently recrystallized in Alpine times. Though garnet (gar_1) in these samples typically contains numerous inclusions, none of them had sufficiently complete inclusion assemblages to warrant thermobarometry. For this reasons, no precise P-T-conditions could be determined for the Permian regional metamorphism.

4.4. ALPINE HIGH PRESSURE OVERPRINT

A group of our samples shows complex zoning in garnet porphyroblasts and characteristic overgrowth textures that document the transition from pre-Alpine to early-Alpine conditions. Typical in metapelites is a mica-rich matrix dominated by white mica – commonly muscovite *and* phengite – but with only subordinate biotite, kyanite overgrowing and partially replacing fibrolite, small and commonly roundish garnet of a a second generation, stubby to long-prismatc staurolite, bands of mosaic quartz with sporadic oligoclase and, in mica-free domains, K-feldspar.

In samples showing tectonite fabrics, however, the high-pressure overprint is extensive and obvious. In Monte Rosa metagranites affected (Dal Piaz and Lombardo, 1986; Frey et al., 1976), phengite has Si-contents of 3.35–3.41 p.f.u., Ti-biotite typically shows $Mg/(Mg+Fe^{2+}) = 0.36 \pm 0.06$, and assemblages include albite + epidote (or oligoclase), microcline, quartz, as well as accessory titanite, garnet, tourmaline, and magnetite. Phengite in metapelites show Si-contents similar to these, except where subsequent exsolution (discussed below) lead to a new generation of low-celadonite micas. Thermobarometric and age data for metagranitoids, based on Frey et al. (1976), are shown in figure 2. Included are only those samples, for which Fe/Mg exchange data for phengite and biotite, as well as oxygen isotope temperatures, indicate the attainment and preservation of equilibrium (i.e. Hunziker, (1970); Hunziker et al., (1992), and this study); pressure values shown for these samples are based on the calibration of Massonne and Schreyer (1987) and Si-values reported by Frey et al. (1976); all ages shown from that study are Rb–Sr isochron results. Results from metabasites studied by Dal Piaz and Lombardo (1986) and Borghi (1996) are also shown. All three studies indicate a low temperature eclogite stage, with preserved equilibria showing mostly 500 ± 50 °C, 10 ± 2 kbar, dated at 35–40 Ma.

In the metapelites we studied, assemblages differ somewhat from eastern to western parts of the Monte Rosa nappe. In the East, two samples from Valle Vigezzo (Po9703 and Bi9801; cf. Figs 1, 5; Tabs 1, 2) deserve detailed characterization:

– Po9703 is a banded, tightly foliated garnet-biotite-muscovite-staurolite-schist sampled NE of Porcella. Grain boundaries are clean and commony straight, aligned monazite grains occur abundantly throughout the matrix that contains recrystallized intergrowths of muscovite and minor biotite. Roundish grains of garnet do not appear to represent more than one generation; similarly pale staurolite is present only in one idiomorphic habitus, as stubby prisms. The Ti-phase is ilmenite only, neither rutile nor titanite have been found. Aluminosilicates are missing, but adjacent samples commonly contain kyanite. TWQ analysis indicates equilibration at conditions close to 600 °C and 10 kbar (Fig. 5) which appear consistent with the assemblage observed, and the field

delimited by the location of equilibria involving kyanite (not shown) includes the three invariant points computed for the observed assemblage. Hence the P-T-result appears credible. Matrix monazite dated from this assemblage indicates an age of 35 ± 2 Ma which is interpreted as the age of equilibration.

– Bi9801 was collected at Alpe Bisoggio, SE of Beura (E of Villadossola) and is very similar to Po9703, both texturally and mineralogically, except that a few larger grains of garnet (gar_1) occur and minor fibrolitic sillimanite (but no kyanite) are observed in the mica-rich matrix. Calculated equilibration conditions (Fig. 5) are shown for mineral compositions excluding siderophyllite equilibria. The remaining three independent reactions indicate similar P-T-conditions, near 600 °C and 11 kbar, reflecting conditions well within the kyanite field. A single monazite grain from a garnet porphyroblast could be extracted and dated, giving an age of 211 ± 47 Ma*, i.e. indicating that gar_1 may represent a Permian relic. Monazite from the matrix occurs in two textural types, as single grains and clusters (SCHERRER et al., 2001a). Our age data indicate recrystallization between 33 ± 1 and 32 ± 1 Ma, and possibly (partial?) resetting at 26 ± 1 Ma. One way to interpret all of these data is to invoke decompression from ≥11 kbar, starting around 34–31 Ma, into the fibrolite field (~5 kbar, assuming isothermal decompression) by 27–25 Ma.

Samples studied from part of the Monte Rosa nappe to the West of Valle d'Ossola include those to the North and South of the upper Val d'Antrona (localities labelled Pz, Ri, Mo; Figs 1, 6, 7; Tabs 1 and 2). Many of these contain overgrowth textures and mineralogical evidence of their polymetamorphic evolution, e.g. chloritoid + kyanite near sillimanite + K-feldspar. Attempts to use TWQ for any of these samples produced highly dispersed patterns with P-T-intersections commonly outside the stability fields of the observed assemblages. Two samples do appear well equilibrated, however:

– Tr9902 is a fine-grained micaschist containing garnet (gar_1) porphyroblasts of >5 mm diameter, sprinkled with tiny inclusions of epidote(?) and with coarse biotite + phengite + quartz in adjacent pressure shadows. Abundant roundish, small grains of garnet (gar_2) with dark cores appear in the mica matrix which contains subordinate quartz, K-feldspar, chlorite, apatite, and rutile rimmed by ilmenite. The matrix and the rock as a whole are not foliated, and the mica assemblage displays pale biotite as rims around muscovite and lamellar patches within coarse white mica. These are interpreted as exsolution features from phengite breakdown (FERRARIS et al., 2000), and the microstructural evidence does not suggest extensive recrystallization during or following that process. Thermobarometric results for three sets of local mineral compositions suggests equilibration conditions between 550–610 °C and 9 ± 2 kbar. The stability field of the observed assemblage and the kyanite-absent field appear to be consistent with the TWQ-intersections, but with only two independent mineral equilibria being usable, the control on the P-T-data is not great. – Monazite occurs both as discrete grains in the matrix and as inclusions in gar_1. Ages obtained for the former indicate a range (from XRF-data only) of 34 ± 8 to 50 ± 17 Ma*, consistent with the only PIMMS date available of 46 ± 2 Ma. Monazite inclusions in early garnet yielded 204 ± 33 and 212 ± 35 Ma* as a maximum age for gar_1 – again seen as evidence of the persistence of Permian (?) garnet. In an adjacent sample (Tr9904) early garnet porphyroblasts contain monazite suggesting an even older age (Tab. 2), as well as xenotime too small to be dated by the techniques used in this study.

– Pz9905 is a staurolite bearing garnet-biotite-white mica gneiss collected on the ridge N of Cime di Pozzuoli. It shows similar characteristics to Tr9902, and despite soome P-T-scatter TWQ indicates similar equilibration conditions as well, 620 ± 60 °C and 9.2 ± 1.8 kbar (Fig. 6). No monazite grains from this sample have been dated, but the consistency between ages obtained for similar samples (Tr9902, Tr9904, and Mo9804) from the NE-portion of the Monte Rosa nappe indicates that these P-T-conditions probably pertain to a similar time segment, i.e. ~40–35 Ma ago.

Phengite breakdown textures such as those described above have been observed in many samples from the northeastern and central parts of the Monte Rosa nappe, including those of the Mo- and Pb-suites (Fig. 1, Tabs 1 and 2). A typical example is shown for Pb9901c (Fig. 6), with pressure-sensitive equilibria scattering broadly for a single assemblage, as well as from one sample or microscopic domain to the next. Fe-Mg exchange equilibria, notably for garnet–biotite, yield far more consistent temperatures, hence it is tempting to regard the scatter in pressure intersections as indicating a possible decompression path. Though no quantitative pressure bounds can be extracted, it may be safe to interpret the P-T patterns for such samples as representing some stages along their Alpine decompression paths. None of the assemblages for which reliable P-T intersection patterns have been documented indicate the preservation of pressures beyond 12 ± 1.5 kbar, but the textures described make it likely that the nappe

had in fact reached somewhat higher pressure conditions previously. The lack of complete recrystallization during the decompression stage may also be responsible for at least part of the dispersion among thermobarometric results of other samples than those described here in detail.

4.5. THERMAL OVERPRINT AND RETROGRADE FEATURES

Many samples from the portion of the Monte Rosa nappe to the East of Valle d'Ossola are dominantly characterized by extensive re-equilibration under medium pressure amphibolite facies conditions, as evidenced by the abundance of muscovite and the appearance of a new generation of idiomorphic staurolite and/or small almandine-rich garnet. Relic phengite is but locally preserved in masses of celadonite-poor muscovite that contain ill defined patches or lamellae of phlogopite in minor amounts (<5%), presumably again due to exsolution from phengite. In more recrystallized samples, such intergrowths developped discrete grain boundaries between muscovite and biotite; thin lamellae (from <1 to 5 μm) of pale biotite are observed even in idiomorphic muscovite grains >200 μm in size. Kyanite is the stable aluminosilicate polymorph, by contrast to some pelites in tectonic units adjacent to the Monte Rosa nappe, especially in eastern parts of Valle Vigezzo and in Centovalli, where sillimanite occurs (NIGGLI and NIGGLI, 1965; TODD and ENGI, 1997). As outlined for sample Bi9801 (see previous section), the Monte Rosa nappe may have been exhumed rapidly enough, such that eastern portion of the nappe experience decompression in the sillimanite field, leading to the local formation of fibrolite (around 26 Ma ago?).

In addition some metapelites show late greenschist facies retrogression, both East and West of Valle d'Ossola. In the former case, this is probably linked to a late imprint after the amphibolite facies thermal maximum, bot outside the Alpine staurolite field, it is impossible to discern two stages. Neither P-T-data not monazite ages interpretable as a specific stage of retrogression could be documented.

5. Implications

5.1. TECTONO-METAMORPHIC EVOLUTION OF THE MONTE ROSA NAPPE

The pre-Variscan metamorphic evolution cannot be defined clearly on the basis of the present results. Sporadic monazite ages found along the southern margin of the nappe (yielding 325 ± 8 Ma in the matrix of Ti9801; 330 ± 8 Ma in An9901 inclusions from texturally old garnet porphyroclasts) agree, within error, with the Rb–Sr isochron age of 310 Ma (±50 Ma according to HUNZIKER, 1970; ±20 Ma according to FREY et al., 1976), interpreted as the age of formation or emplacement of the Monte Rosa granodiorite pluton. Present knowledge, unfortunately, does not constrain the depth of emplacement of this major magmatic body. The isolated garnet grains containing the oldest monazite dated here are interpreted as contact-metamorphic in origin.

The late Variscan phase of magmatism, dated by HUNZIKER (1970) and HUNZIKER and BEARTH (1969) at 260 ± 10 Ma, produced lesser but widespread volumes of granitic magmas. Permian contact metamorphism is thought to have caused well equilibrated assemblages to form in metapelites such as the Za-suite described in this study. In most samples of that suite sillimanite and K-feldspar are abundant, and only samples demonstrably affected by the Alpine event contain texturally younger kyanite, an approximate pressure bracket of 5 ± 2 kbar may be estimated for the intrusive activity around 260 Ma. Monazite grains from many garnet porphyroblasts and a few matrix assemblages, covering a very large portion of the Monte Rosa nappe, indicate ages within error of this magmatic phase. It appears likely, therefore, that one cannot separate the thermal effects of contact metamorphic from those of a regional metamorphic phase with associated penetrative deformation (HUNZIKER, 1970; HUNZIKER and BEARTH, 1969). In view of the indicated intrusive depth of 10–20 km, advective heating during the extended Variscan magmatic activity may well have raised the geothermal gradient regionally. Upper amphibolite facies assemblages, such as those documented in the present study, including restitic migmatite portions, would thus have possibly resulted from partial melting during that phase. This is not to suggest that the granitic magmatism in this unit at that time resulted from in-situ partial melting, but the absence of thermal aureoles, the paucity of skarn-like features, and the high grade overprint evident in metapelites at least suggest a close link in space and time.

For the Alpine time period, no early subduction-related prograde metamorphism is evident in metapelites, except possibly in a few chloritoid-bearing assemblages in the central part of the nappe (e.g. Za 9705). It seems unlikely that the P-T-t-relations derived from the Alpine assemblages correspond to the deepest subduction stage, given the widespread evidence of phengite (par-

tial) breakdown observed. Probably, partial re-equilibration occurred during ascent or extrusion of the Monte Rosa nappe. Remarkably, however, the pressures obtained are almost always around 9–11 kbar, and for a time segment near 35–40 Ma. No significant regional pressure gradient could be documented for the exhumation stage (Fig. 8), nor is a regional age progression discernible, within the uncertainty of the available data for that stage (Fig. 3d) of the Monte Rosa thrust sheet.

Whether the higher pressures found by CHOPIN and MONIÉ (1984) and LE BAYON et al. (2001) reflect marginal fragments of the thrust sheet that attained somewhat deeper levels, or whether these conditions reflect the (maximum?) depth reached by the entire nappe, is not clear at the moment. The temperatures obtained in these two studies (~500 °C) are remarkably low, compared to our thermometric results. One certainly cannot rule out the possibility of substantial heating during emplacement of the thrust sheet to mid-crustal levels (e.g. BROUWER, 2000; ENGI et al. 2001), but it is also possible that fragmentation of the Monte Rosa nappe occurred in the subduction channel, with some parts reaching greater depth. Evidence for deep extrusion of fragments is available from the ultra-high pressure (UHP) conditions reported from the nearby Lago di Cignana area (REINECKE, 1998; VAN DER KLAUW et al., 1997).

In samples taken to the East of Valle d'Ossola, the Barrovian overprint is strong and has traditionally been assumed to have obliterated most of the earlier high-pressure effects. However, the P-T-conditions indicated by the best-equilibrated of the samples presented in this study indicate a clear discrepancy to the Barrovian conditions (TODD and ENGI, 1997) established for metapelites of adjacent tectonic units (Fig. 8), for which pressures are at least 2–3 kbar lower. Assuming that the conditions documented by the multi-equilibrium thermobarometry correspond approximately to T_{max} and $P(T_{max})$, this discrepancy in pressure indicates that the Monte Rosa nappe reached its T_{max}-conditions during emplacement into the surrounding units, and somewhat earlier (i.e. at a deeper level) than these. Because the temporal constraints are not tight for this phase in adjacent units, no precise inference on the dynamics of emplacement can be derived. However, the emplacement suggests a tempting explanation for the remarkable "protrusion" of the isotherms (FREY et al., 1999) to the SW of the Lepontine dome, in that the rapid extrusion of the Monte Rosa nappe may have introduced advective heat and possibly generated additional shear heating. This heat source would then have perturbed the simple geometry of the regional thermal anomaly depicted by the isotherm pattern further east (ENGI et al., 1995; TODD and ENGI, 1997). The temporal constraints available for the transition from high-pressure to Barrovian conditions in the Monte Rosa nappe certainly permit such an interpretation.

Relevant in this respect are also recent age data by ROMER et al. (1996) for a suite of dykes from eastern parts of the Monte Rosa nappe,

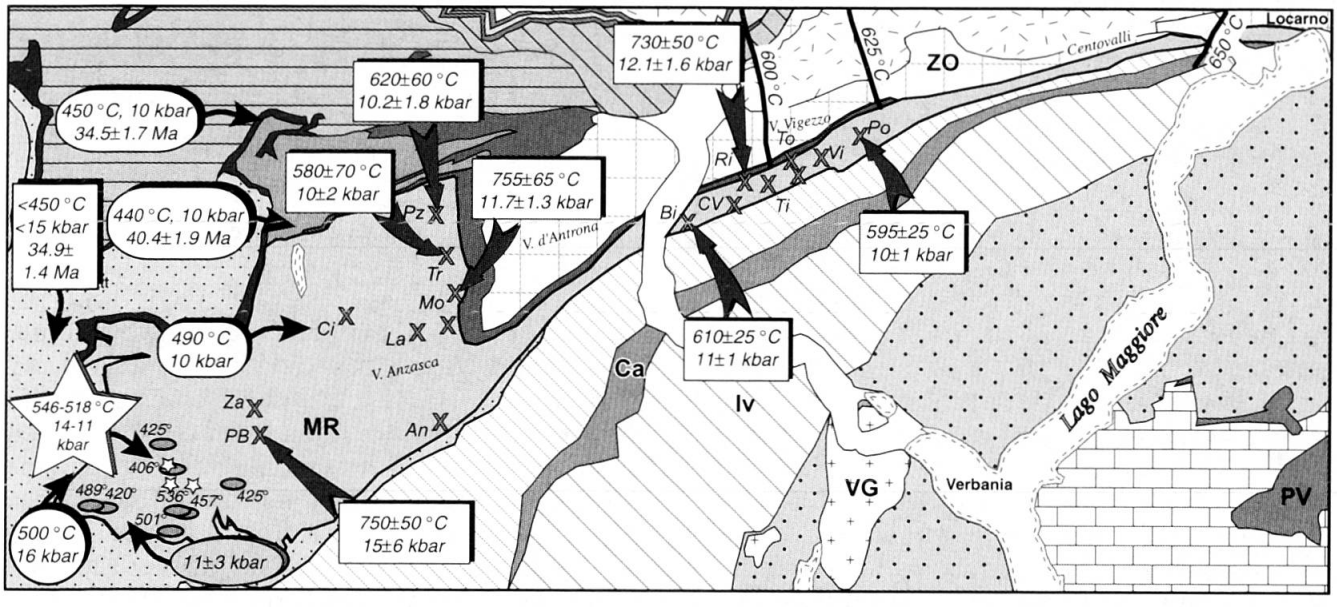

Fig. 8 Comparison of metamorphic conditions derived for Alpine high-pressure (exhumation) stage in present study of metapelites, with data from the literature for other rock types. New data shown in rectangular boxes with broad arrows indicating sample locations; other symbols as in Fig. 2.

which were very accurately dated for two localities. U–Pb ages were obtained from zircon at 30 to 28 Ma, and from xenotime at 26 Ma, all interpreted as dating the postkinematic emplacement of late magmatic aplites and pegmatites under waning metamorphic conditions.

5.2. BEHAVIOUR OF METAPELITES AND MONAZITE WITHIN THESE DURING POLYMETAMORPHISM

One of the samples studied retains only Permian characteristics, presumably because it was not exposed to significant deformation or fluid-rock interaction during the Alpine cycle. In this case, both the assemblage of the rock forming minerals (see previous section) and the U–Th–Pb system in monazite are interpreted as having preserved a Variscan state (Tab. 2). These are remarkable results, as there is no doubt that these samples experienced subsequent subduction to at least lower crustal depth, involving reheating to 550–650 °C and rapid extrusion in a convergent setting. We note that the classical study by KÖPPEL and GRÜNENFELDER (1975) reported dates on monazite separates from Monte Rosa granite and one of the metapelites (from Camplicciolì), and that both of these gave U–Pb ages of 260 ± 5 Ma!

Many other samples retain partial Permian characteristics, including undisturbed monazite in porphyroblasts and –clasts, even where matrix recrystallization caused complete resetting of the monazite grains in the micaschist portion of these samples. Rather few monazite grains indicate "mixed" ages, presumably due to old cores or domains having been overgrown by Alpine monazite. Such intragrain zoning in monazite has commonly been visualized by means of backscatter images in the EMP, and the main chemical cause is due to heterogeneity in Th contents. However, because EMP techniques are inadequate to date young monazite chemically (the limit being <100–200 Ma, depending on Th contents), and the spatial resolution of the μ-XRF and LA-ICPMS instruments is insufficent to resolve different age zones (Fig. 3) in single grains of the size available, "mixed ages" cannot be avoided in some cases (SCHERRER et al., 2001a).

The occurrence of old monazite inclusions in garnet is best explained if the garnet cores are also assumed to be of Permian age. This hypothesis is supported by chemical zoning patterns observed in some of the large garnet grains that show a homogeneous core surrounded by one or more growth rims (chemical profile in Fig. 4). We thus think that the cores of such garnet grains are Permian in age, with the rim being due to Alpine metamorphism. It is not impossible, of course, that the entire garnet might be Alpine in age, but with its core portion simply having included old monazites. This interpretation would require garnet growth at an early Alpine stage prior to the recrystallization of monazite. Because garnet shows a compositional change between core and the overgrowth rim, the Alpine growth of garnet would have had to be polyphase. The observed zoning patterns are thus more in agreement with a Permian origin.

Even in a sample with strong retrogression (Ti9801), monazite in a garnet retains a Permian age, whereas monazite in the chlorite-mica matrix yield mixed ages (Tab. 2; Fig. 2). The preservation of Permain monazites in matrix (see also sample Za9702), as well as the occurrence of mixed ages in a "Alpine" chorite-mica matrix indicate that the presence of fluid and certain metamorphic conditions are not the only factors controlling the "resetting" of monazite. A process related to growth and/or recrystallization of monazites are necessary to reset the monazite. Understanding monazite forming reactions is needed to use such data in deciphering the P-T-t evolution. Reactions of monazite are indicated by symplectites described in SCHERRER et al. (2001b) and can be also inferred from element compositions. For example, zoning patterns of yttrium in monazite, with enriched cores and depleted rims within the heterogeneous grains, support the observation and idea put forward by PYLE and SPEAR (1999) and FOSTER et al. (2000), i.e. that high yttrium monazite growth precedes garnet growth, whereas monazite growing after garnet nucleation tends to be depleted in yttrium. Xenotime has been observed in a few samples of the metapelite suite investigated here, but its grain size is insufficient for single grain dating by the methods employed.

6. Conclusions

New P-T-t data have been derived from the polymetamorphic basement rocks of the Monte Rosa nappe. 'In-situ' micro-dating of monazite by PIMMS and μ-XRF technology combined with thermobarometry has been successfully applied to improve the understanding of the complex polymetamorphic history of the Monte Rosa nappe. Two distinct phases of monazite growth emerged, first in the Permian (around 260 Ma ago), related to the intrusion of the Monte Rosa granite; then during Alpine orogeny, around 35 Ma ago, associated with high pressure metamorphism during Tertiary subduction/obduction.

As in other internal units of the Eastern, Central, and Western Alps, a prominent high pressure phase of Alpine age has been documented in the Monte Rosa nappe, reaching eclogite facies conditions during a narrowly constrained period of 40–35 Ma. The record is remarkably similar to that in the adjacent Zermatt-Saas Fee zone, to the Adula nappe, Cima Lunga complex, and the Mergoscia-Arbedo zone further East, and to the Gran Paradiso and Dora Maira further to the Southwest. These units show substantial differences in the internal structure, rock contents, and their pre-Alpine evolution. Similarities in the tectonic and temporal setting of the Alpine metamorphism does, however, suggest a coherent Alpine evolution. The present study contributes new constraints for its reconstruction. Given the present tectonic situation of the Monte Rosa nappe with respect to the Southern Steep Belt and the Insubric Line, it appears that this lineament, or its precursor, acted as a guiding structural element in the hangingwall of the Alpine subduction channel, along which the nappe stack was exhumed. Unlike the highly fragmented and internally attenuated character of other units extruded from eclogite facies depth, such as the Adula nappe, the Cima Lunga complex, and the Mergoscia-Arbedo zone including Alpe Arami (ENGI et al., 2001), the Monte Rosa nappe shows that a rather massive, coherent tectonic body could be also exhumed along this same channel within the same time segment and, most likely, a similar overall transpressional regime.

We conclude that the Alpine subduction channel acted as a conduit for extrusion not only of highly attenuated fragments, as in the case of the Southern Steep Belt of the Alps (ENGI et al., 2001), but also to guide the exhumation of rather more massive upper crustal fragments from depths >40 km back to upper crustal levels.

Acknowledgements

Access to and support at the facilities of NIGL Nottingham, U.K., was made possible by Randy Parrish and is gratefully acknowledged. Discussions with Christian Chopin, Alfons Berger, and Giorgio Dal Piaz have helped us clarify our own thinking. Comments from Lukas Baumgartner improved the presentation. This study has been supported by Schweizerischer Nationalfonds (Credit 20-49671.96/1 and 2000-055306.98/1), as has the EMP laboratory at the MPI Bern (Credit 21-26579.89).

References

ARGAND, E. (1911): Les nappes de recouvrement des Alpes Pennines et leurs prolongements structuraux. Matériaux pour la Carte Géol. Suisse; nouv. série, 31.

BEARTH, P. (1939): Über den Zusammenhang von Monte Rosa- und Bernhard-Decke. Eclogae geol. Helv. 32(1), 101–111.

BEARTH, P. (1952): Geologie und Petrographie des Monte Rosa. Beitr. Geol. Karte Schweiz, Neue Folge 96. Liefg., 94.

BEARTH, P. (1958): Über einen Wechsel der Mineralfazies in der Wurzelzone des Penninikums. Schweiz. Mineral. Petrogr. Mitt. 38, 363–373.

BERMAN, R.G. (1991): Thermobarometry using multi-equilibrium calculations: a new technique, with petrological applications. Can. Mineral. 29, 833–855.

BERMAN, R.G. and ARANOVICH, L.Y. (1996): Optimized standard state and mixing properties of minerals: I. Model calibration for olivine, orthopyroxene, cordierite, garnet, and ilmenite in the system FeO–MgO–CaO–Al_2O_3–SiO_2–TiO_2. Contrib. Mineral. Petrol. 126, 1–24.

BORGHI, A., COMPAGNONI, R. and SANDRONE, R. (1996): Composite P-T paths in the internal Penninic massifs of the western Alps: Petrological constraints to their thermo-mechanical evolution. Eclogae geol. Helv. 89(1), 345–367.

BROUWER, F.M. (2000): Thermal evolution of high-pressure metamorphic rocks in the Alps. Doctoral thesis, Utrecht University, 146 pp.

CHOPIN, C. and MONIÉ, P. (1984): A unique magnesio-chloritoid-bearing, high-pressure assemblage from the Monte Rosa, Western Alps; petrologic and ^{40}Ar–^{39}Ar radiometric study. Contrib. Mineral. Petrol. 87, 388–398.

COMPAGNONI, R. and MAFFEO, B. (1973): Jadeite-bearing metagranites s.l. and related rocks in the Mount Mucrone area (Sesia-Lanzo Zone, western Italian Alps). Schweiz. Mineral. Petrogr. Mitt. 53, 355–378.

DAL PIAZ, G.V. (1964): Il cristallino antico del versante meridionale del Monte Rosa. Paraderivati a prevalente metamorfismo alpino. Rend. Soc. It. Min. Petr. 20, 101–136.

DAL PIAZ, G.V. (1966): Gneiss ghiandoni, marmi ed anfiboliti antiche del ricroprimento Monte Rosa nell'alte Val d'Ayas. Boll. Soc. Geol. It. 85, 103–132.

DAL PIAZ, G.V. (1971): Nuovi ritrovamenti di cianite alpina nel cristallino antico del Monte Rosa. Rend. Soc. It. Min. Petr. 27(2), 437–477.

DAL PIAZ, G.V. (2001): Geology of the Monte Rosa massif: historical review and personal comments. Schweiz. Mineral. Petrogr. Mitt. 81, 275–303.

DAL PIAZ, G.V. and LOMBARDO, B. (1986): Early Alpine eclogite metamorphism in the Penninic Monte Rosa-Gran Paradiso basement nappes of the northwestern Alps. In: EVANS, B. W. and BROWN, E. H. (eds): Blueschists and eclogites. Geol. Soc. Am. Mem. 164, 249–265.

DAL PIAZ, G.V. and LOMBARDO, B. (1995): Alpine Tectonics and Metamorphism of the Western Alps. Guidebook for the Pre-Symposium Field Excursion. In: VII Internat. Symp. Antarctic Earth Sci., Siena (Italy), 61 pp.

DUCHÊNE, S., BLICHERT-TOFT, J., LUAIS, B., TELOUK, P., LARDEAUX, J.M. and ALBAREDE, F. (1997): The Lu-Hf dating of garnets and the ages of the Alpine high-pressure metamorphism. Nature 387, 586–589.

ELLIS, D.J. and GREEN, D.H. (1979): An experimental study of the effect of Ca upon garnet-clinopyroxene exchange equilibria. Contrib. Mineral. Petrol. 71, 13–22.

ENGI, M., BERGER, A. and ROSELLE, G.T. (2001): The role of the tectonic accretion channel (TAC) in a collisional orogen. Geology 29, number 12.

ENGI, M., TODD, C.S. and SCHMATZ, D.R. (1995): Tertiary metamorphic conditions in the eastern Lepontine

Alps. Schweiz. Mineral. Petrogr. Mitt. 75(3), 347–369.

FERRARIS, C., GROBÉTY, B. and WESSICKEN, R. (2000): Phlogopite exsolutions within muscovite: a first evidence for a higher-temperature re-equilibration, studied by HRTEM and AFM techniques. Europ. J. Mineral. 13, 15–26.

FOSTER, G., KINNY, P., VANCE, D., PRINCE, C. and HARRIS, N. (2000): The significance of monazite U–Th–Pb age data in metamorphic assemblages; a combined study of monazite and garnet chronometry. Earth Planet. Sci. Lett. 181, 327–340.

FRANCHI, S. (1903): Sul rinvenimento di nuovi giacimente di roccie giadeitiche nelle Alpi occidentali e nell'Appennino ligure. Boll. Soc. Geol. It. 22, 130–134.

FREY, M., DESMONS, J. and NEUBAUER, F. (1999): The new metamorphic map of the Alps. Schweiz. Mineral. Petrogr. Mitt. 79, 1–230.

FREY, M., HUNZIKER, J.C., O'NEIL, J.R. and SCHWANDER, H. (1976): Equilibrium-disequilibrium relations in the Monte Rosa granite, Western Alps: Petrological, Rb–Sr and stable isotope data. Contrib. Mineral. Petrol. 55, 147–179.

FREY, M. and FERREIRO MÄHLMANN, R. (1999): Alpine metamorphism of the Central Alps. Schweiz. Mineral. Petrogr. Mitt. 79, 135–154.

FROITZHEIM, N. (2001): Origin of the Monte Rosa nappe in the Pennine Alps – A new working hypothesis. Geol. Soc. Am. Bull. 113, 604–614.

GEBAUER, D. (1999): Alpine geochronology of the Central and Western Alps: new constraints for a complex geodynamic evolution. Schweiz. Mineral. Petrogr. Mitt. 79, 191–208.

HUNZIKER, J. C. (1970): Polymetamorphism in the Monte Rosa, Western Alps. Eclogae geol. Helv. 63(1), 151–161.

HUNZIKER, J.C. and BEARTH, P. (1969): Rb–Sr-Altersbestimmungen aus den Walliser Alpen; Biotitalterswerte und ihre Bedeutung für die Abkühlungsgeschichte der alpinen Metamorphose. Eclogae geol. Helv. 62, 205–222.

HUNZIKER, J.C., DESMONS, J. and HURFORD, A.J. (1992): Thirty-two years of geochronological work in the Central and Western Alps; a review on seven maps. Mém. Géol. Lausanne vol. 13.

HUNZIKER, J.C. and MARTINOTTI, G. (1984): Geochronology and evolution of the Western Alps: a review. Mem. Soc. Geol. It. 29, 43–56.

KRETZ, R. (1983): Symbols for rock-forming minerals. Am. Mineral. 68, 277–279.

KÖPPEL, V. and GRÜNENFELDER, M. (1975): Concordant U–Pb ages of monazite and xenotime from the Central Alps and the timing of high temperature metamorphism, a preliminary report. Schweiz. Mineral. Petrogr. Mitt. 55, 129–132.

KÖPPEL, V., GÜNTHERT, A. and GRÜNENFELDER, M. (1981): Patterns of U–Pb zircon and monazite ages in polymetamorphic units of the Swiss Central Alps. Schweiz. Mineral. Petrogr. Mitt. 61, 97–120.

KROGH, E. J. (1988): The garnet-clinopyroxene Fe-Mg geothermometer – a reinterpretation of existing experimental data. Contrib. Mineral. Petrol. 99, 44–48.

LANGE, S., NASDALA, L., POLLER, U., BAUMGARTNER, L. P. and TODT, W. (2000): Crystallization age and metamorphism of the Monte Rosa Granite, Western Alps. In: 17th Swiss Tectonic Studies Group Meeting, ETH Zürich, p. 51.

LE BAYON, R., SCHMID, S.M. and DE CAPITANI, C. (2001): The metamorphic evolution of the Monte Rosa nappe and its relation to exhumation by fore- and back-thrusting in the Western Alps. Geol. Paläont. Mitt. Innsbruck, 25, 132–133.

LIATI, A., GEBAUER, D., FROITZHEIM, N. and FANNING, M. (2001): U–Pb SHRIMP geochronology of an amphibolitized eclogite and an orthogneiss from the Furgg zone (Western Alps) and implications for its geodynamic evolution. Schweiz. Mineral. Petrogr. Mitt. 81, 379–393.

MASSONNE, H.-J. and SCHREYER, W. (1987): Phengite geobarometry based on the limiting assemblage with K-feldspar, phlogopite, and quartz. Contrib. Mineral. Petrol. 96, 212–224.

MASSONNE, H.-J. and SZPURKA, Z. (1997): Thermodynamic properties of white micas on the basis of high-pressure experiments in the systems K_2O–MgO–Al_2O_3–SiO_2–H_2O and K_2O–FeO–Al_2O_3–SiO_2–H_2O. Lithos 41, 229–250.

MATTIROLO, E., NOVARESE, V., FRANCHI, S. and STELLA, A. (1913): Carta Geologica d'Italia, Foglio 29 Monte Rosa (1:100'000), Serv. Geol. Ital.

MONIÉ, P. (1985): La methode ^{39}Ar–^{40}Ar appliquée au metamorphisme alpin dans le massif du Mont-Rose (Alpes occidentales); chronologie detaillée depuis 110 Ma. Eclogae geol. Helv. 78, 487–516.

NAGEL, T. (2000): Metamorphic and structural history of the southern Adula nappe (Graubünden, Switzerland). Unpub. Ph.D. Thesis, University of Basel, Basel.

NAGEL, T., DE CAPITANI, C. and FREY, M. (2001): Isograds and PT-evolution in the eastern Lepontine Alps, Switzerland. J. Metamorphic Geol. 19, nr. 6.

NIGGLI, E. (1970): Alpine Metamorphose und alpine Gebirgsbildung. Fortschr. Mineral. 47, 16–26.

NIGGLI, E. and NIGGLI, C. (1965): Karten der Verbreitung einiger Mineralien der alpidischen Metamorphose in den Schweizer Alpen (Stilpnomelan, Alkali-Amphibol, Chloritoid, Staurolith, Disthen, Sillimanit). Eclogae geol. Helv.,58, 335–368.

OBERHÄNSLI, R., HUNZIKER, J.C., MARTINOTTI, G. and STERN, W.B. (1985): Geochemistry, geochronology and petrology of Monte Mucrone: an example of eo-alpine eclogitization of Permian granitoids in the Sesia-Lanzo zone, western Alps, Italy. Chem. Geol. 52, 165–184.

PAQUETTE, J.-L., CHOPIN, C. and PEUCAT, J.-J. (1989): U–Pb zircon, Rb–Sr and Sm–Nd geochronology of high- to very-high-pressure meta-acidic rocks from the western Alps. Contrib. Mineral. Petrol. 101, 280–289.

PARRISH, R.R. (1990): U–Pb dating of monazite and its application to geological problems. Canad. J. Earth Sci. 27, 1431–1450.

PAWLIG, S. and BAUMGARTNER, L.P. (2001): Geochemistry of a talc-kyanite-chloritoid shear zone within the Monte Rosa granite, Val d'Ayas, Italy. Schweiz. Mineral. Petrogr. Mitt. 81, 329–346.

PETTKE, T., DIAMOND, L. and VILLA, I. (1999): Mesothermal gold veins and metamorphic devolatilisation in the NW Alps: The temporal link. Geology 27, 641–644.

PFIFFNER, M. and TROMMSDORFF, V. (1998): The high-pressure ultramafic-mafic-carbonate suite of Cima Lunga-Adula, Central Alps: Excursions to Cima di Gagnone and Alpe Arami. Schweiz. Mineral. Petrogr. Mitt. 78, 337–354.

PYLE, J.M. and SPEAR, F.S. (2000): An empirical garnet (YAG) – xenotime thermometer. Contrib. Mineral. Petrol. 138, 51–58.

REINECKE, T. (1998): Prograde high- to ultrahigh-pressure metamorphism and exhumation of oceanic sediments at Lago di Cignana, Zermatt-Saas Zone, western Alps. Lithos, 42(3–4), 147–189.

REINHARDT, B. (1966): Geologie und Petrographie der Monte-Rosa Zone, der Sesia-Zone und des Canavese im Gebiet zwischen Valle d'Ossola und Valle Loana. Schweiz. Mineral. Petrogr. Mitt., 46, 553–678.

ROMER, R. L., SCHÄRER, U. and STECK, A. (1996): Alpine and pre-Alpine magmatism in the root-zone of the western central Alps. Contrib Mineral Petrol. 123(2), 138–158.

ROSELLE, G.T., THÜRING, M. and ENGI, M. (2002): MELONPIT: A finite element code for simulating tectonic mass movement and heat flow within subduction zones. Am. J. Sci., in press.

RUBATTO, D. and GEBAUER, D. (1999): Eo/Oligocene (35 Ma) high-pressure metamorphism in the Gornergrat Zone (Monte Rosa, Western Alps): implications for paleogeography. Schweiz. Mineral. Petrogr. Mitt. 79, 353–362.

SCHERRER, N.C., ENGI, M., GNOS, E., JAKOB, V. and LIECHTI, A. (2000): Monazite analysis; from sample preparation to microprobe age dating and REE quantification. Schweiz. Mineral. Petrogr. Mitt. 80, 93–105.

SCHERRER, N.C., ENGI, M., CHEBURKIN, A., PARRISH, R.R. and BERGER, A. (2001a): Non-destructive chemical dating of young monazite using XRF: 2. Context sensitive microanalysis and comparison with Th–Pb laser-ablation mass spectrometric data (LA-PIMMS). Chem. Geol. (accepted for publication).

SCHERRER, N.C., GNOS, E. and CHOPIN, C. (2001b): A retrograde monazite-forming reaction in bearthite-bearing high-pressure rocks. Schweiz. Mineral. Petrogr. Mitt. 81, 369–378.

SPICHER, A. (1980): Tektonische Karte der Schweiz, 1:500'000, Schweizerische Geologische Kommission.

STECK, A., BIGIOGGERO, B., DAL PIAZ, G.V., ESCHER, A., MARTINOTTI, G. and MASSON, H. (2001): Carte tectonique des Alpes de Suisse occidentale et des régions avoisinantes, 1:100'000. Serv. hydrol. géol. nat., Carte spéc. no. 123, 4 maps.

TODD, C.S. (1998): Limits to GASP-thermobarometry in Ca-poor rocks such as metapelites. Am. Mineral. 83, 1161–1167.

TODD, C. S. and ENGI, M. (1997): Metamorphic field gradients in the Central Alps. J. Metamorphic. Geol. 15(4), 513–530.

VAN DER KLAUW, S.N.G.C., REINECKE, T. and STOCKHERT, B. (1997): Exhumation of ultrahigh-pressure metamorphic oceanic crust from Lago di Cignana, Piemontese zone, western Alps: the structural record in metabasites. Lithos 41(1–3), 79–102.

ZINGG, A. and HUNZIKER, J.C. (1990): The age of movements along the Insubric Line West of Locarno (northern Italy and southern Switzerland). Eclogae geol. Helv. 83, 629–644.

Manuscript received June 25, 2001; revision accepted September 15, 2001.
Editorial handling: L.P. Baumgartner

Appendix

MINERAL REACTIONS USED IN TWQ THERMOBAROMETRY

Refers to Fig. 5

Sample: Po9703b **3 linearly independent reactions**
TWQ results: P = 10.0 ± 1.0 kbar T = 595 ± 25 °C
Reactions
2): 2 Alm + 2 Msp + Phl = 3 Sd + 6 aQz + Py
3): 3 FSt + 4 Phl + 8 Msp + 4 Alm = 24 aQz + 12 Sd + 3 MSt
4): 4 Ann + 3 MSt = 3 FSt + 4 Phl
5): 2 Msp + Ann + Alm = 6 aQz + 3 Sd
6): Alm + Phl = Py + Ann
9): Py + 2 Msp + 2 Ann = Phl + 6 aQz + 3 Sd
15): 3 FSt + 2 Py + 2 Phl + 4 Msp = 12 aQz + 6 Sd + 3 MSt
16): 3 FSt + 4 Py + 8 Msp + 4 Ann = 24 aQz + 12 Sd + 3 MSt

Sample: Bi9801a **3 linearly independent reactions**
TWQ results: P = 11.0 ± 1.0 kbar T = 610 ± 25 °C
Reactions
1): Alm + Ann + 2 Msp = 3 Sd + 6 aQz
2): 6 FSt + 5 Phl + 30 Msp + 46 Ann = 3 Clh + 117 aQz + 81 Sd
3): 2 Ann + 2 Msp + Py = 3 Sd + 6 aQz + Phl
4): 53 Ann + 10 Phl + 12 FSt = 45 Sd + 18 Msp + 6 Clh + 39 Alm
5): 62 Msp + 3 Clh + 46 Alm = 5 Phl + 159 aQz + 57 Sd + 6 FSt
6): 27 Alm + 3 Clh + 24 Msp = 6 FSt + 45 aQz + 5 Phl + 19 Ann
7): 31 Ann + 5 Phl + 6 FSt = 36 Sd + 27 aQz + 3 Clh + 15 Alm
8): Alm + Phl = Py + Ann
9): 2 Alm + 2 Msp + Phl = 3 Sd + 6 aQz + Py
10): 14 Ann + 49 Phl + 12 FSt = 45 Sd + 39 Py + 18 Msp + 6 Clh
11): 12 Sd + 23 Py + 16 Msp + 3 Clh = 28 Phl + 21 aQz + 6 FSt
12): 6 FSt + 5 Py + 40 Msp + 56 Ann = 3 Clh + 147 aQz + 96 Sd
13): 8 Ann + 3 Clh + 24 Msp + 27 Py = 6 FSt + 45 aQz + 32 Phl
14): 16 Ann + 20 Phl + 6 FSt = 36 Sd + 27 aQz + 15 Py + 3 Clh
15): 12 FSt + 63 Phl + 14 Alm = 6 Clh + 18 Msp + 53 Py + 45 Sd
16): 49 Alm + 6 Clh + 18 Msp + 45 Sd = 12 FSt + 10 Py + 63 Ann
17): 56 Alm + 3 Clh + 72 Msp = 6 FSt + 72 Sd + 189 aQz + 5 Py
18): 8 Alm + 3 Clh + 24 Msp + 19 Py = 6 FSt + 45 aQz + 24 Phl
19): 6 FSt + 36 Phl + 16 Alm = 3 Clh + 31 Py + 27 aQz + 36 Sd
20): 32 Alm + 3 Clh + 24 Msp = 6 FSt + 45 aQz + 5 Py + 24 Ann
21): 6 FSt + 5 Py + 36 Ann = 20 Alm + 3 Clh + 27 aQz + 36 Sd

Refers to Fig. 6

Sample: Pz9905b **3 linearly independent reactions**
TWQ results: P = 9.2 ± 1.8 kbar T = 620 ± 60 °C
Reactions
5): Alm + Ann + 2 Msp = 3 Sd + 6 aQz
8): 3 Alm + 6 mcel = 3 Sd + 18 aQz + 2 Phl + Ann
12): 5 Alm + 6 mcel = 3 Sd + 18 aQz + 2 Py + 3 Ann
13): 3 Sd + 3 mcel = 2 Ann + 3 Msp + Phl
14): 4 Ann + 5 Msp + Py = 6 Sd + 6 aQz + 3 mcel
17): 2 Ann + 6 mcel + 3 Py = 3 Sd + 18 aQz + 5 Phl
18): 2 Alm + Msp + 3 mcel = 3 Sd + 12 aQz + Phl
19): Alm + 3 mcel = 6 aQz + Phl + Msp + Ann
20): 3 Sd + 3 mcel + Alm = 3 Ann + 3 Msp + Py
21): 4 Alm + 3 Msp + 3 mcel = 6 Sd + 18 aQz + Py
22): 2 Alm + 3 mcel = 6 aQz + Py + Msp + 2 Ann
24): Alm + Phl = Py + Ann
25): 2 Alm + 2 Ms + Phl = 3 Sd + 6 aQz + Py
26): Py + 6 mcel + 2 Alm = 3 Phl + 18 aQz + 3 Sd
27): 3 mcel + Py = 6 aQz + 2 Phl + Msp
28): 2 Ann + 2 Msp + Py = 3 Sd + 6 aQz + Phl
29): 3 Sd + 2 Py + 3 mcel = 2 Alm + 3 Msp + 3 Phl
30): 2 Alm + 2 Msp + Phl = 3 Sd + 6 aQz + Py

Sample: Pb9901c **3 linearly independent reactions**
TWQ results: P(1) = 17–21 kbar T(1) = 770 ± 30 °C
P(2) = 9–12 kbar T(2) = 730 ± 30 °C
Reactions
3): Alm + Ann + 2 Msp = 3 Sd + 6 aQz
5): 3 mcel + Alm = Ann + Ms + Phl + 6 aQz
6): 6 mcel + 3 Alm = Ann + 2 Phl + 18 aQz + 3 Sd
9): 5 Alm + 6 mcel = 3 Sd + 18 aQz + 2 Py + 3 Ann
11): 3 Py + 6 mcel + 2 Ann = 5 Phl + 18 aQz + 3 Sd
12): 2 Alm + Msp + 3 mcel = 3 Sd + 12 aQz + Phl
13): 3 mcel + Alm = Ann + Msp + Phl + 6 aQz
14): 4 Alm + 3 Msp + 3 mcel = 6 Sd + 18 aQz + Py
15): 2 Alm + 3 mcel = 6 aQz + Py + Msp + 2 Ann
16): Phl + Alm = Ann + Py
18): 2 Alm + 6 mcel + Py = 3 Sd + 18 aQz + 3 Phl
19): Py + 2 Msp + 2 Ann = Phl + 6 aQz + 3 Sd
20): 2 Alm + 2 Msp + Phl = 3 Sd + 6 aQz + Py

Refers to Fig. 7

Sample: Mo9801c **3 linearly independent reactions**
TWQ results: P = 11.7 ± 1.3 kbar T = 755 ± 65 °C
Reactions
1): 2 Msp + Ann + Alm = 6 aQz + 3 Sd
2): 6 mcel + 3 Alm = Ann + 2 Phl + 18 aQz + 3 Sd
3): 6 mcel + 5 Alm = 3 Ann + 2 Py + 18 aQz + 3 Sd
4): 3 mcel + 3 Sd = Phl + 3 Msp + 2 Ann
5): 2 Alm + Msp + 3 mcel = 3 Sd + 12 aQz + Phl
6): Alm + 3 mcel = 6 aQz + Phl + Msp + Ann
7): Alm + 3 mcel + 3 Sd = Py + 3 Msp + 3 Ann
8): 4 Alm + 3 Msp + 3 mcel = 6 Sd + 18 aQz + Py
9): Py + 5 Msp + 4 Ann = 3 mcel + 6 aQz + 6 Sd
10): 2 Alm + 3 mcel = 6 aQz + Py + Msp + 2 Ann
11): Phl + Alm = Ann + Py
12): Py + 6 mcel + 2 Alm = 3 Phl + 18 aQz + 3 Sd
13): 3 Py + 6 mcel + 2 Ann = 5 Phl + 18 aQz + 3 Sd
14): 3 mcel + 2 Py + 3 Sd = 3 Phl + 3 Msp + 2 Alm
15): Phl + 2 Msp + 2 Alm = Py + 6 aQz + 3 Sd
16): Py + 3 mcel = Msp + 2 Phl + 6 aQz
17): Py + 2 Msp + 2 Ann = Phl + 6 aQz + 3 Sd

Sample: Ri9801b **(left) 4 linearly independent reactions**
TWQ results: P = 12.1 ± 1.6 kbar T = 735 ± 55 °C
Reactions
1): Alm + Ann + 2 Msp = 3 Sd + 6 aQz
2): Msp + Ab = Pg + Kfs
3): 3 Sd + 3 mcel = 2 Ann + 3 Msp + Phl
4): 4 Ann + 5 Msp + Py = 6 Sd + 6 aQz + 3 mcel
5): Alm + Ann + 2 Pg + 2 Kfs = 3 Sd + 6 aQz + 2 Ab
6): 2 Alm + Msp + 3 mcel = 3 Sd + 12 aQz + Phl
7): Alm + 3 mcel = 6 aQz + Phl + Msp + Ann
8): 3 Alm + 6 mcel = 3 Sd + 18 aQz + 2 Phl + Ann
9): 3 Sd + 3 mcel + Alm = 3 Ann + 3 Msp + Py
10): 4 Alm + 3 Msp + 3 mcel = 6 Sd + 18 aQz + Py
11): 2 Alm + 3 mcel = 6 aQz + Py + Msp + 2 Ann
12): 5 Alm + 6 mcel = 3 Sd + 18 aQz + 2 Py + 3 Ann
13): 3 Sd + 3 mcel + 3 Ab = 2 Ann + 3 Pg + Phl + 3 Kfs
14): 4 Ann + 5 Pg + 5 Kfs + Py = 6 Sd + 6 aQz + 3 mcel + 5 Ab
15): 3 mcel + Py = 6 aQz + 2 Phl + Msp
16): 2 Ann + 2 Msp + Py = 3 Sd + 6 aQz + Phl
17): 2 Ann + 6 mcel + 3 Py = 3 Sd + 18 aQz + 5 Phl
18): 2 Alm + 3 mcel + Pg + Kfs = 3 Sd + 12 aQz + Phl + Ab
19): Ab + Alm + 3 mcel = 6 aQz + Kfs + Phl + Pg + Ann
20): 3 Sd + 3 mcel + Alm + 3 Ab = 3 Ann + 3 Pg + 3 Kfs + Py
21): 4 Alm + 3 mcel + 3 Pg + 3 Kfs = 6 Sd + 18 aQz + Py + 3 Ab
22): Ab + 2 Alm + 3 mcel = 6 aQz + Py + Kfs + Pg + 2 Ann
23): 3 Sd + 2 Py + 3 mcel = 2 Alm + 3 Msp + 3 Phl
24): Alm + Phl = Py + Ann
25): 2 Alm + 2 Msp + Phl = 3 Sd + 6 aQz + Py
26): 2 Alm + 6 mcel + Py = 3 Sd + 18 aQz + 3 Phl
27): Ab + 3 mcel + Py = 6 aQz + Kfs + 2 Phl + Pg
28): 2 Ann + 2 Pg + 2 Kfs + Py = 3 Sd + 6 aQz + Phl + 2 Ab
29): 3 Sd + 2 Py + 3 mcel + 3 Ab = 2 Alm + 3 Pg + 3 Phl + 3 Kfs
30): 2 Alm + 2 Pg + Phl + 2 Kfs = 3 Sd + 6 aQz + Py + 2 Ab

Sample: Ri9801c **(right)3 linearly independent reactions**
TWQ results: P = 12.0 ± 1.5 kbar T = 730 ± 50 °C
Reactions
1): Alm + Ann + 2 Msp = 3 Sd + 6 aQz
2): 3 Sd + 3 mcel = 2 Ann + 3 Msp + Phl
3): 4 Ann + 5 Msp + Py = 6 Sd + 6 aQz + 3 mcel
4): 2 Alm + Msp + 3 mcel = 3 Sd + 12 aQz + Phl
5): Alm + 3 mcel = 6 aQz + Phl + Msp + Ann
6): 3 Alm + 6 mcel = 3 Sd + 18 aQz + 2 Phl + Ann
7): 3 Sd + 3 mcel + Alm = 3 Ann + 3 Msp + Py
8): 4 Alm + 3 Msp + 3 mcel = 6 Sd + 18 aQz + Py
9): 2 Alm + 3 mcel = 6 aQz + Py + Msp + 2 Ann
10): 5 Alm + 6 mcel = 3 Sd + 18 aQz + 2 Py + 3 Ann
11): 3 mcel + Py = 6 aQz + 2 Phl + Msp
12): 2 Ann + 2 Msp + Py = 3 Sd + 6 aQz + Phl
13): 2 Ann + 6 mcel + 3 Py = 3 Sd + 18 aQz + 5 Phl
14): 3 Sd + 2 Py + 3 mcel = 2 Alm + 3 Msp + 3 Phl
15): Alm + Phl = Py + Ann
16): 2 Alm + 2 Msp + Phl = 3 Sd + 6 aQz + Py
17): 2 Alm + 6 mcel + Py = 3 Sd + 18 aQz + 3 Phl